Chem Soc Rev

Recent advances in automotive catalysis for NOx emission control by small-pore microporous materials

Journal:	*Chemical Society Reviews*
Manuscript ID:	CS-REV-02-2015-000108.R1
Article Type:	Review Article
Date Submitted by the Author:	14-Apr-2015
Complete List of Authors:	Szanyi, Janos; Pacific Northwest National Laboratory, Institute for Integrated Catalysis Peden, Charles; Pacific Northwest National Laboratory, Institute for Integrated Catalysis Gao, Feng; Pacific Northwest National Lab., Chemical & Materials Sciences Division Beale, Andrew; University College London, Department of Chemistry; Utrecht University, Inorganic Chemistry and Catalysis Lezcano-Gonzales, Ines; University College London, Chemistry

Recent advances in automotive catalysis for NO_x emission control by small-pore microporous materials

A. M. Beale[1,2], F. Gao[3], I. Lezcano-Gonzalez[1,2], C.H.F. Peden[3] and J. Szanyi[3]

[1] Department of Chemistry, University College London, 20 Gordon Street, London WC1H 0AJ, UK

[2] UK Catalysis Hub, Research Complex at Harwell, Rutherford Appleton Laboratory, Didcot, OX11 0FA, UK

[3]Institute for Integrated Catalysis, Pacific Northwest National Laboratory, Richland, WA, USA

Abstract

The ever increasing demand to develop highly fuel efficient engines coincides with the need to minimize air pollution originating from the exhaust gases of internal combustion engines. Dramatically improved fuel efficiency can be achieved at air-to-fuel ratios much higher than stoichiometric. In the presence of oxygen in large excess, however, traditional three-way catalysts are unable to reduce NOx. Among the number of lean-NOx reduction technologies, selective catalytic reduction (SCR) of NOx by NH3 over Cu- and Fe-ion exchanged zeolite catalysts has been extensively studied over the past 30+ years. Despite the significant advances in developing a viable practical zeolite-based catalyst for lean NOx reduction, the insufficient hydrothermal stabilities of the zeolite structures considered cast doubts about their real-world applicability. During the past decade a renewed interest in zeolite-based lean NOx reduction was spurred by the discovery of the very high activity of Cu-SSZ-13 (and the isostructural Cu-SAPO-34) in the NH3 SCR of NOx. These new, small-pore zeolite-based catalysts not only exhibited very high NOx conversion and N2 selectivity, but also exhibited exceptional high hydrothermal stability at high temperatures. In this review we summarize the key discoveries of the past ~5 years that lead to the introduction of these catalysts into practical application. The review first briefly discusses the structure and preparation of the CHA structure-based zeolite catalysts, and then summarizes the key learnings of the rather extensive (but not complete) characterisation work. Then we summarize the key findings of reaction kinetics studies, and provide some mechanistic details emerging from these investigations. At the end of the review we highlight some of the issues that still need to be addressed in automotive exhaust control catalysis.

Content:

1. Introduction

The abatement of environmentally harmful compounds (e.g., hydrocarbons (HC), oxides of nitrogen (NO_x) and sulfur (SO_x), and CO), emitted from mobile or stationary power sources, has been a remarkable success story for the catalysis R&D community.[1] In particular, for mobile (automotive exhaust emission control) applications, the "three-way" catalyst that is the active component of the "catalytic converter", a standard component on vehicles in the US and Europe

for over 30 years, has contributed to a remarkable drop in emissions of CO, HC and NO_x from gasoline-powered vehicles. We now take for granted the dramatic improvements that the introduction of the catalytic converter technology has made in air quality and, correspondingly, human health.

Unfortunately, the "three-way" catalytic converter technology is not suitable for application on so-called "lean-burn" engines that operate at high air/fuel ratios, including diesel-powered vehicle engines. Although these engine technologies are inherently more fuel efficient than "stoichiometric" gasoline powertrains, their wide-spread application for vehicles has been limited by the inability of the three-way catalyst to reduce NO_x emissions at high air/fuel ratios. As such, in the last 10-15 years a significant R&D focus has been on this problem of "lean-NO_x" emission control.[2-8] Based on this recent work, significant achievements have been realized with the very recent commercialization of two new nano-materials-based catalytic emission control applications for diesel-powered vehicles: the NO_x storage/reduction (NSR) catalyst and the selective catalytic reduction with ammonia (NH_3-SCR) using metal-exchanged zeolites. Because these are such newly introduced technologies, many challenges remain to improve performance, enhance stability, and lower costs. Indeed, many of the practical concerns with these new "lean-NO_x" catalyst technologies stem from a relatively poor fundamental understanding of catalyst structure/activity and reaction mechanisms.

In this review, we summarize the results of recent studies of zeolite-based catalysts for the SCR of NO_x using NH_3 as the reductant. First we will give an overview of the development of zeolite-based SCR catalysts, then briefly discuss the most important parameters of the CHA-based zeolite synthesis protocol, and provide key structural information of these materials. In the following section we will summarize the key findings of the extensive characterization work that

have appeared over the past ~5 years on Cu- and Fe-SSZ-13 catalysts. This will be followed by a section detailing the key findings of kinetic studies over these materials and present some of the mechanistic proposals based on both the structural characterization and detailed kinetic measurements. Finally we present some of the future challenges we are facing in the field of automotive exhaust control catalysis.

1.1. Development of metal-exchanged zeolites for vehicle applications

The development of SCR using metal-exchanged zeolite catalysts for automotive applications is by no means an isolated event. Prior to zeolite catalysts, a wide variety of other materials, e.g., supported noble metals, coinage metal oxides and salts, and early transition metal oxides have been examined.[9-11] The identification of ammonia as a particularly efficient reductant for NO_x removal even dates back to the 1950s.[12] The most relevant and useful prior knowledge comes from the development of oxide supported vanadia SCR systems for stationary NO_x removal applications (e.g., in coal-fired power plants), initiated in Japan in the early 1970s and adopted worldwide at present.[10, 11] Our understanding of fundamental SCR chemistry on zeolite catalysts also largely originates from studies on supported vanadia catalysts [10]. As a result of the considerable experience with vanadia-based SCR catalysts in stationary applications, it has been under consideration for vehicle applications for quite some time and, in fact, this catalyst system has been commercialized in Europe.[13] Due to concerns in the U.S. about vanadia wastes from production activities as well as issues with low hydrothermal durability, low activity/selectivity outside its optimal operational temperature window, and undesired activity in catalyzing SO_2 oxidation to SO_3 of these catalysts, metal-exchanged zeolites are now being more widely used for vehicle NH_3-SCR applications.

The discovery and development of the zeolite-based SCR catalysts are relatively recent, having occurred over the last 25+ years. In 1986, Iwamoto and coworkers published a milestone paper[14] describing high and stable activity of Cu^{2+} exchanged ZSM-5 in NO decomposition to N_2 and O_2. This was followed by a surge of research interest in NO decomposition which, in fact, would be an ideal reaction for NO_x removal as it does not require a secondary reductant.[2] It was soon realized, however, that the efficiency of this process was so low that practical application for catalytic NO decomposition was not likely. In fact, Schneider and coworkers have demonstrated on thermodynamic grounds that such a process could not meet emission standards for lean-burn engines [15]. Investigations of Cu-ZSM-5 as an SCR catalyst with hydrocarbon or NH_3 reductants began in the early 1990s, and interest in these materials quickly heightened due to the comparable, and in certain cases superior performance for "fresh" Cu-ZSM-5 as compared to the commercialized vanadia-titania SCR catalysts.[12, 16-19] In particular, the use of hydrocarbons as reductants (HC-SCR) received special interest because hydrocarbons are readily available in the exhaust from incomplete combustion of fuels.[17] Unfortunately, it was soon realized that that Cu-ZSM-5 deactivates rapidly under hydrothermal conditions typically encountered in practical vehicle exhaust environments.[20, 21]

Due partly to the need for more durable zeolite-based catalysts, but mostly due to the need for more efficient hydrocarbon activation in HC-SCR, Fe-ZSM-5 became the next research focus. The hydrothermal stabilities were, indeed, somewhat improved, especially for ZSM-5 based catalysts formulated with high Fe loadings.[22-27] However, the durability of these Fe-ZSM-5 materials was still not satisfactory for practical vehicle applications. Furthermore, it was becoming clear during this time that SCR with NH_3 over these zeolite-based catalysts provided significantly better performance for NO_x reduction than HC-SCR.[28, 29]

Subsequently, Cu- and Fe-beta for NH_3-SCR have been extensively studied because they show better durability than ZSM-5 based catalysts.[30-35] Still, there were concerns that metal-exchanged beta zeolites would not maintain their high activities to meet the regulated durability requirements (100,000 miles or more in the U.S. standards)[36]. Another practical concern with these candidate SCR catalysts became apparent with testing in real engine exhaust [36]. Notably, some of the exhaust hydrocarbons from incompletely burned fuel appeared to act as catalyst poisons in part because they strongly adsorb in zeolites. Periodic high temperatures encountered on the vehicle can also lead to the highly exothermic combustion of the adsorbed hydrocarbons resulting in locally very high temperatures sufficient to degrade the zeolite structure.

1.2. Metal-exchanged CHA zeolites

It seems likely that the issues with unburned hydrocarbons in large-pore beta zeolites may have motivated the exploration of small-pore materials. Prior to the development of Cu-containing CHA-type materials for SCR applications, H-SAPO-34 (i.e. a silicoaluminophosphate material isostructural to SSZ-13 zeolite) has been successfully used as a commercial methanol-to-olefin catalyst.[37, 38] To our knowledge, however, the SSZ-13 zeolite has never been widely used as an industrial catalyst. While both materials show strong Brønsted acidity, experimental[39, 40] as well as theoretical studies[41] seem to suggest that H-SSZ-13 displays stronger acidity. In any case, metal-exchanged CHA-type microporous materials were developed simultaneously by BASF and Johnson-Matthey Inc. in the mid- to late-2000s for lean-NO_x NH_3 SCR in Diesel-powered vehicles.[42-45] These CHA-based catalysts, first commercialized for NO_x emission control in 2010, are now the most common choice for SCR of NO_x with NH_3 (provided by urea solutions) in vehicle applications. CHA zeolites (structural model is shown in Fig. 1) have been known since the 1950s[46], and viable synthesis procedures for SSZ-13 were invented

by Stacy Zones at Chevron in the mid-1980s.[47] The very recent reports of their improved performance for NH_3-SCR relative to metal-exchanged ZSM-5 and beta[42, 43, 48] has sparked considerable interest in and debate about the fundamental materials and chemical properties of these metal-exchanged CHA zeolites. The remainder of this review will focus mainly on what has been learned, primarily over the last five years, and what is currently proposed about Cu-CHA zeolites with regard to their structure and catalytic chemistry for NH_3-SCR. The much less studied Fe-CHA SCR catalysts will also be described, although in less details.

2. Cu(Fe)-CHA Synthesis

SSZ-13 is readily synthesized hydrothermally. Detailed synthesis recipes based on the original Zones patent[47] can be found in the recent literature[49-51], in which, *N*,*N*,*N*-trimethyl-1-adamantamonium iodide/hydroxide have been chosen as structure directing agents (SDA). The hydroxide form is commercially available from Sachem, Inc. In principle, the chabasite structure can be constructed with Si/Al ratios from 1 to infinity. By varying Si/Al ratios of the precursor, one can readily synthesize SSZ-13 with various Si/Al ratios. It is important to note that Si/Al ratio is an important criterion for determining kinetics, stability and catalyst operating window for Cu-SSZ-13 catalysts. To accommodate sufficient amounts of Cu^{2+} ions and to ensure sufficient hydrothermal stability, the current generation of commercial Cu-SSZ-13 catalyst has a Si/Al ratio of ~15[52]. Cu-SSZ-13 is readily generated via a traditional aqueous solution ion-exchange method that has also been described in detail in recent publications.[48-51, 53] SAPO-34 is also synthesized hydrothermally using a vast number of organic and inorganic Al and Si sources and SDAs (alkylamines and morpholine). Previous studies have discovered the following important parameters that affect the properties of synthesized SAPO-34: (1) the SDA chosen; (2) the Al and Si sources; (3) the molar ratios of Si/Al/P/SDA of the gel; (4) gel aging

time/temperature; (5) reaction time/temperature.[54-59] Among these, SDAs play decisive roles in affecting crystallite size, Si distribution and, therefore, framework charge density, while the choice of inorganic Al and Si sources and maintaining continuous stirring during synthesis is important to form products with high crystallinity. The presence of three tetrahedral elements (instead of two for zeolites) and the possible existence of silica islands within SAPO-34 make this material intrinsically more complex than SSZ-13. Cu-SAPO-34 can also be generated via the traditional solution ion-exchange method. Note that although calcined SAPO-34 is in the H-form, to facilitate Cu^{2+} ion incorporation, it is still necessary to exchange it into the NH_4-form.[59-61] Furthermore, the generation of Cu-SAPO-34 from this method is not trivial due to the moisture sensitivity of this material at temperatures lower than 100 °C [59, 62-64]. Fe-CHA can be prepared similarly using NH_4-CHA and solution of a Fe(II) salt; however, care must be taken to avoid Fe^{2+} oxidation to Fe^{3+} which leads to bulky Fe-complexes (i.e. iron oxyhydroxides) during ion exchange. This was achieved by N_2 protection during ion exchange, which is discussed in more details elsewhere.[65]

A few alternative Cu-CHA synthesis methods were developed in the past a few years. Ren et al. discovered that Cu^{2+}–tetraethylenepentamine complex (Cu–TEPA), owing to its stability, proper size and charge-balancing nature, can be used as a SDA for "one-pot" Cu-SSZ-13 synthesis.[66] There is, unfortunately, a clear drawback when Cu–TEPA is used alone as the SDA: in the final product, the Cu content can readily be too excessive, because multiple SDA molecules are required to generate one CHA unit cell. As will be shown below, excessive Cu loading is detrimental to the hydrothermal stability of Cu-CHA. To lower the Cu content, a "reverse" ion-exchange step is required to remove some of the Cu^{2+} ions.[67] It is important to note that this approach avoids the expensive traditional SDAs for SSZ-13 synthesis. Cu–TEPA was

also found to be an efficient SDA for one-pot Cu-SAPO-34 synthesis. In this case, it can be used as a co-SDA, together with other low cost SDAs, to allow Cu loadings to be readily controlled.[68, 69] Another method successfully used to synthesize Cu-CHA is a so-called solid-state ion exchange (SSIE) method. For example, heating up a CuO and SSZ-13/SAPO-34 mixture to an elevated temperature (700 °C and above) allows for formation of extra-framework Cu^{2+} according to the following reactions:[70, 71]

$$2H^+ + CuO = Cu^{2+} + H_2O \quad (1)$$

$$H^+ + CuO = [Cu(OH)]^+ \quad (2)$$

This method is rather straightforward and allows facile Cu loading control. However, incomplete CuO reaction and partial damage of the zeolites at such high temperatures are the drawbacks. Very recently, Shwan et al discovered that NH_3 and/or a standard NH_3-SCR feed allows SSIE at much lower temperatures (250 °C).[72] The mobility of Cu at low temperatures has been proposed to be related to the formation of $[Cu^{I}(NH_3)_x]^+$ ($x \geq 2$) complexes.

3. Characterisation of Cu-CHA

3.1. X-ray techniques

X-rays have a long standing history in the characterisation of heterogeneous catalysts by their virtue of being highly penetrative thereby allowing sample interrogation under appropriate conditions relevant to heterogeneous catalysis (etc. correct gas composition, temperature and more recently pressure).[73] The principle techniques that have been used to characterize ion-exchanged CHA catalysts to date are X-ray diffraction and X-ray absorption spectroscopy at the K-edges which for Cu and Fe are found at 8977 and 7120 eV, respectively, and in many cases during the SCR reaction (defined as being under *operando* conditions when catalytic activity is verified using a residual gas analyser i.e. a mass spectrometer) Much less studied (in general) are

the L-edges for these elements which are too low in energy to allow for facile in situ interrogation.

As with all K-edge spectroscopy, it is possible to obtain detailed insight into the local environment of Cu in terms of both coordination (number and to some extent ligand-type) and oxidation state which for Cu is dominated by 0, +1 and +2. The tendency for the 4s ground state to remain unoccupied often results in XANES spectra with multiple resonances. For the investigation of Cu-CHA materials X-ray techniques have been primarily employed to identify the nature and type of Cu-containing species during all stages of the catalyst lifetime i.e. from characterising the material before, during and after reaction.

3.1.1. XANES

It is known that after calcination and exposure to the atmosphere Cu-CHA materials contain $[Cu(H_2O)_6]^{2+}$ species that are Jahn-Teller distorted. Evidence for the presence of this species can be seen in a typical Cu K-edge XANES by virtue of a weak pre-edge feature around 8977 eV due to a 1s-3d ($^2T_{2g}$) transition which since $\Delta l > 1$, is dipole forbidden but quadrupole allowed; the transition is especially weak since it is also forbidden on symmetry grounds by virtue of the Cu coordination possessing a centre of inversion (either Oh or else if the Jahn-Teller distortion is very strong D4h) as well as a reduced transition probability by virtue of the d^9 electronic configuration. In contrast, a weak pre-edge peak results in a strong intensity of the rising absorption edge since, importantly, this transition between the 1s to the unoccupied 4p is both dipole and parity (symmetry) allowed; around and even beyond this point the spectral features become dominated by multiple scattering around the absorber as a consequence of the low mean free path of the excited electron; the more neighbours around the absorber the more intense the multiple scattering and the sharper the features. Interestingly then the intensity of the

rising absorption edge (in conjunction with the change in the pre-edge peak intensity) is a quick indicator of the coordination around Cu species in zeolites having been shown to reduce in intensity as the coordination number decreases, particularly the formation of 'undercoordinated' Cu species.[74] Heating of Cu-CHA leads to progressive dehydration of Cu which results in an increase in the intensity of the pre-edge peak and simultaneous decrease of the white line, both changes characteristic of a reduction in the coordination number as the dehydrated Cu^{2+} ions adopt specific positions in the framework with a lower symmetry. An illustration of the changes in the XANES data as this process occurs is given in Figure 2 where, in addition to the changes in the pre-edge peak and white line, a newly appearing pre-edge shoulder assigned to 1s/4p transitions in the 8985–8990 eV range and the Cu^{2+} fingerprint peak at ca. 8977.5 eV which is also consistent with a less symmetric Cu coordination geometry.[51, 75, 76]

XANES has also been used to detect the presence of Cu oxides (Cu_xO_y) – notably Bates et al. demonstrated the presence of these additional species by virtue of a pre-edge feature at 8987 eV within samples whereby the Cu/Al_{tot} atomic ratio > 0.2; importantly for XANES data, corresponding evidence for a secondary species could also be found in the form of a reduced white line intensity. At low concentrations this can be more easily observed when examining 1st derivative XANES spectra.[77]

XANES is also sensitive to a change in the ligand type around the absorber; for example, a change from all O ligands to N ligands in $[Cu(NH_3)_4]^{2+}$ results in a spectrum containing a dip in white line intensity with two features appearing at 8994 eV and 8998 eV respectively.[78] These features have even been observed under pre-SCR conditions and where it has also been proposed as evidence for NH_3 adsorption on the Cu site at low temperatures during standard SCR.[51] The pre-edge position of Cu^+ was also shown to be sensitive to its coordination environment. The

pre-edge energy of Cu^+ with adsorbed CO shifted to lower energy by about 1.5 eV in comparison to the adsorbate-free Cu^+ ion.[75]

A second notable pre-edge feature pertinent to the understanding of Cu behaviour under SCR conditions is the observation of a feature at ~ 8982 eV and is thought to be due to a transition from a 1s to the doubly degenerate $4p_{xy}$ orbitals in two-coordinate Cu^+ systems. This feature is very evident in the data reported by Deka et al. in Cu-SSZ-13 samples prepared via a CVD method which resulted in the formation of significant amounts of $CuAlO_2$ and consequently large amounts of unwanted N_2O in the NH_3-SCR reaction of NO.[79] Significant amounts of Cu^+ were also observed in the study by Kispersky et al. whom studied Cu-SSZ-13 and Cu-ZSM-5 under standard SCR conditions and concluded from a linear combination fitting of reference spectra that the greater extent of Cu reduction seen in Cu-ZSM-5 (65 % Cu^+ vs. 15 % Cu^+ in Cu-SSZ-13) could explain its greater overall deNOx activity at 200 °C. [52, 80] A similar follow-up study by Bates et al., this time examining the impact of Si:Al on the nature of the Cu active sites, also observed a similar general redox trend with lower Si:Al ratios leading to a greater extent of Cu^+ formation at 180 °C using a similar gas composition (see Figure 3). From these studies as well as those by Deka et al. and Borfecchia et al. it appears that the extent of reduction shows a strong temperature dependency and that heating Cu-SSZ-13 under standard SCR reaction conditions above 200 °C and below 300 °C, a region of maximum NO conversion, only Cu^{2+} species have thus far been observed. Very few studies have moved beyond 300 °C since above this temperature Cu-CHA samples tend to burn NH_3 resulting in reduced NO consumption.

For the most part XANES has very much been used as a fingerprint technique, however with the advent of photon in-photon out techniques such as high resolution fluorescence

detection (HERFD) or else valence-to-core (V2C) X-ray emission spectroscopy it is now possible to resolve many more of the features that contribute to an XANES spectrum, thereby enabling more detailed structural insight (i.e. information concerning the local environment around an absorber).[81] However in order to fully appreciate this resolution it is often necessary to employ Density Functional Theory (DFT) to produce reliable energy-minimised structural models from which a spectral simulation can be attempted. This combination has the potential then to resolve subtle differences in the spectra such as might be expected if there were a change in ligand type from Cu-$O_{(framwework)}$ to Cu-OH and ultimately to tackle a mixture of Cu species in different coordination and oxidation states; as in the work of Borfecchia et al. for example where both Cu^{+} and Cu^{2+} were observed to occupy both the 6 ring (6R) and the 8 rings (8R) although the amounts of each species present in each position differed.[76] X-ray emission spectroscopy in combination with EXAFS (and IR) has been used to propose that after calcination in O_2/He that the Cu^{2+} located on the 8R is actually a $[Cu(OH)]^{+}$ species.[76]

3.1.2. EXAFS

Analysis of the EXAFS data from Cu is normally dominated by the first shell, near neighbor (NN) contributions although the preference for site occupancy in one or two positions means that unlike with Cu-ZSM-5 or beta, a more detailed (multiple shell) structure analysis can be performed; hence in the work by Korhonen et al. it was possible to identify the close location of the Cu ions in the proximity of the CHA framework immediately after calcination.[7, 82] Of particular interest is the observation of an 'undercoordinated' (3 coordinate) Cu^{2+} species in calcined samples as a result of the Cu species tendency to locate in the corners of the 6R that makes up the double 6 ring (D6R) that link the large cages in the zeolite structure (see Fig. 1). Importantly this reduction in site symmetry is also confirmed by XANES and also by

examination of the Debye-Waller factor which also suggests the Cu species sites exhibit little static or thermal disorder and are therefore very much ensconced into the 6R. Evidence for a fourth coordinating ligand is difficult to verify since the ligand would typically be some ~ 2.7 Å for the Cu centre across the 6R which also coincides with the contributions from the zeolite framework. It should also be noted that there remains the possibility that Cu ions might simultaneously reside in both 6Rs that make up the D6R and that this could be one conceivable origin of the Cu_xO_y clusters/dimeric species recently reported to be also present in addition to the single Cu ions. More recently Borfecchia et al. proposed that after calcination and cooling to room temperature in O_2/He a similar 3 coordinate Cu^{2+} species is observed although this time located in the 8R of the zeolite cage with two Cu-$O_{(cage)}$ linkages and a Cu-OH ligand.

Hydrated Cu^{2+} species initially present as $[Cu(H_2O)_6]^{2+}$ in calcined and air-exposed Cu/CHA samples are Jahn-Teller distorted. If the distortion is strongly tetragonal it becomes very difficult to determine the presence of axial coordination since these distances can be very long and are likely masked by a combination of the zeolite framework and at certain distances, their scattering contribution is often anti-phasic to that of the equatorial ligands.[83] As such, for the most part, EXAFS analysis of the principle component in the Fourier Transform is confined to yielding Cu-NN information on the equatorial ligands which is marginally sensitive to distinguishing between Cu^{2+}-O and the longer Cu^{2+}-N coordination.[84]

Reduction of Cu^{2+} species to Cu^{+} appears difficult to detect unambiguously with EXAFS, particularly if only partial reduction occurs. Nominally a good indicator for a reduction with the retention of neighbour type is a lengthening of the Cu-NN distance – however in the case of Cu^{+} the filled $3d^{10}$ electronic configuration means that Cu^{+} compounds are often two coordinate and linear resulting in a reduction in both Cu coordination and bond length.[52] XANES then appears

to be much more sensitive to the formation of reduced Cu species although since XANES data are collected immediately before the EXAFS (depending on the acquisition mode which if in Quick EXAFS one can consider that the data are essentially simultaneous) one can verify the results of the former against the latter and perform a comparative linear combination analysis of the XANES/Vegard analysis of the EXAFS to estimate the proportion of Cu species present.[52, 85]

3.1.3. X-ray Diffraction

3.1.3.1. In situ

The advantage with diffraction techniques is that they offer mean 'atomic' resolution of structures through reciprocal space. The disadvantage when studying Cu loaded systems is that the low-loading of Cu (~2 % wt.) typical of the most catalytically interesting Cu-CHA materials makes it challenging to unambiguously assign electron density to certain species, particularly when studied under reaction conditions. This has a particular importance for ion-exchanged zeolite systems such as SSZ-13, in that the cationic species tend to significantly populate only at a couple of sites in the micropore volume as shown in Figure 4, although, it has been remarked that the number of potential cationic positions in SSZ-13 is much greater than this. The extent of occupation of these sites by Cu ions however depends on the temperature of the system, the degree of hydration of the cationic species (as well as likely the oxidation state). For example it was first shown by Fickel and Lobo that the occupancy of Cu^{2+} species in the plane of the 6R increases with calcination (in air) temperature such that on reaching a maximum of 450 °C all Cu species can be accounted for in this position.[86] As has been shown however, this position is an average of Cu positions which can be considered to occupy 3 'corners' of the 6R.[82] Similar behaviour was observed by Deka at al. under standard SCR conditions in which with increasing operational temperature Cu was seen to gradually migrate into the plain of the 6R and which

coincided with maximum conversion of NO.[51] A recent study by Andersen et al. using maximum entropy methods on fully dehydrated Cu-SSZ-13 at room temperature was able to observe the location of a Cu species in the 8R (as well as in the 6R) which the authors, in combination with DFT, suggested could be the $[Cu^{2+}(OH)^{-}]^{+}$ complex proposed/observed in the recent combined spectroscopy/DFT studies.[76, 87]

3.1.3.2. *Ex situ*

Although, this technique is used primarily for phase identification it is also clear that there are some notable differences/characteristics in the nature of the SSZ-13 sample which appear to correlate with activity. For example, multiple exchanges and calcination procedures tend to lead to a sharpening of the Bragg peaks and therefore improved crystallinity and to better activity.[88] Powder XRD has also been used to illustrate that CHA contains, almost without exception, intergrowths of AEI although the significance of this on catalytic activity has yet to be conclusively explored for deNOx although there is potential scope here judging by some recent material in the patent literature. [89-91] XRD has also been useful to confirm deactivation of the CHA catalysts either through partial loss of crystallinity through poisoning or else via that long exposure to high temperatures (~ 800 °C) and 10 % (vol.) water vapour content (hydrothermal aging) leads to a complete loss of microporous structure. [77, 92]

3.2. Optical spectroscopies

3.2.1. UV-Vis

The advantage that UV-Vis spectroscopy has over X-ray techniques is its ability to interrogate samples containing many different metal species (i.e. zeolites) and when using fiber optic technology up to working temperatures of 700 °C. [93] The technique has been used principally to characterize Cu-CHA materials during dehydration and in one instance during

SCR. The $[Cu(H_2O)_6]^{2+}$ in calcined and air-exposed Cu-CHA that gives rise to its pale-blue colour is characterised by a broad and asymmetric absorption in the UV-Vis spectrum around 12,000 cm^{-1} in the visible part of the spectrum and is due to a ^2E_g and $^2T_{2g}$ transition; the asymmetry arising due to the Jahn-Teller distortion which can sometimes be resolved into three sub-components at ~ 12400, 11500 and 10700 cm^{-1} which likely correspond to transitions originating from d(xz), d(yz) $\rightarrow$ d(x^2-y^2), d(xy) $\rightarrow$ d(x^2-y^2) and d(z^2) $\rightarrow$ d(x^2-y^2). Substitution of O-based ligands for N-based ligands which have stronger ligand field strength results in a shift in the absorption to a higher wavenumber. [84] In addition to d–d transitions, an intense absorption band centered at around 48,000 cm^{-1} due to ligand-to-metal charge transfer (LMCT) transition is observed.[94]

On dehydration, the sample colour changes from pale blue to an intense dark blue which is manifested in the UV-Vis spectrum as a strong, blue-shifted absorption in the visible part of the spectrum, consistent with a drop in symmetry/coordination (becoming less Laporte forbidden) around the Cu^{2+} environment. Conversely there is a clear red shift of the LMCT band consistent with a change in ligand type from ionic Cu-(OH_2) in $[Cu(H_2O)_6]^{2+}$ to covalent Cu-$O_{(framework)}$. Interestingly the UV-Vis data contained additional resonances at 29,000 and 19,700 cm^{-1} which has been proposed to be due to the presence of either planar or bis(μ-η^2:η^2 peroxo) dicopper species ($[Cu_2(\mu\text{-}\eta^2\text{:}\eta^2\text{-}O_2]^{2+}$) – see Figure 5. No bis(μ-oxo)dicopper species, which are known to be readily present in Cu-ZSM-5 and which have been shown active for NO decomposition, have been detected in Cu-CHA samples to date. However, 'bulk-like' CuO species have been detected at high Cu loadings brought about by multiple ion exchange or low Si:Al and which tend to be observed around 35000 – 40000 cm^{-1}.[77, 94] Interestingly it may be that

these species are the same Cu_xO_y species observed for SSZ-13 catalysts possessing high NO_x oxidation activity, often considered to be the rate determining step in deNOx SCR processes.[95]

3.2.2. IR Spectroscopy

Due to its wide applicability and availability, IR spectroscopy is a commonly used method for zeolite characterisation. It provides detailed structural information of the zeolite framework vibrations, cation vibrations, extra-framework species and hydroxyl groups, and can be applied under either *in situ* or *in operando* conditions. Furthermore, IR spectroscopy of adsorbed probe molecules, such as NO, CO, NH_3 or pyridine, can be employed to characterise adsorption sites in zeolites. Upon adsorption, the vibrational spectra of probe molecules change, providing information on surface sites. Nowadays, a variety of IR techniques, such as transmission-absorption, attenuation total reflection, diffuse reflectance or photoacoustic spectroscopy, are available. Nevertheless, due to its relative simplicity and wide applicability, transmission and diffuse reflectance spectroscopies are frequently used in zeolite characterisation and catalysis.

3.2.2.1. IR Spectroscopy of adsorbed CO

CO is a widely used probe molecule for IR spectroscopic studies of zeolites, especially because of its weak basicity, small molecular diameter and the high sensitivity of the C-O stretching frequency to the environment. It is well established that the carbonyl stretching mode responds to coordination onto Lewis metal sites leading to frequency shifts. Moreover, the C-O stretch is also sensitive to H-bonding to hydroxyl groups, so it can be employed to investigate zeolite Brønsted acidity. Regarding the characterisation of Cu-containing zeolites, CO is commonly used to probe the oxidation state of Cu ions; i.e. whereas Cu^+ ions are able to form

carbonyl complexes, Cu^{2+}(CO) species are very unstable and are difficult to detect. Recent reviews regarding the use of CO as a probe molecule can be found elsewhere.[96-98]

IR spectroscopy of adsorbed CO has been used to determine the nature of the Cu ions present in Cu-SSZ-13. Characterisation of zeolite samples with different ion exchange levels showed the appearance of two vibrational features of CO adsorbed on Cu^+ (2155 and 2135 cm^{-1}), suggesting the presence of two different cationic positions for Cu^+ ions.[99] The samples were annealed in vacuum at 400 ºC for 2 h, so CO was used to probe the Cu^+ species formed during the activation treatment, wherein auto-reduction of Cu^{2+} ions occur.[99] These results were further confirmed by studies on Cu-SSZ-13 samples submitted to different pre-treatments and thus, with different populations of Cu^{2+} and Cu^+ ions.[100, 101]

Szanyi et al. used CO adsorption to characterise Cu-SSZ-13 zeolites annealed in vacuum, oxidised or else reduced with CO and then annealed in vacuum, though almost no differences were observed in the spectra recorded after the different pre-treatments.[100] As seen in Figure 6, at low CO coverage, the spectra recorded for the reduced sample exhibited the features characteristic of CO adsorbed on Cu^+ ions (2154 and 2135cm^{-1}), while increasing CO coverage resulted in the formation of dicarbonyl species (2178 cm^{-1} and increase and red-shift of the band at 2154 cm^{-1}). Moreover, a low intensity feature was also observed in the reduced sample at 2220 cm^{-1}, assigned to Cu^{2+}-CO species. Note however, that both dicarbonyl and Cu^{2+}-CO species were only formed in the presence of excess of gas-phase CO, and their stabilities were very low. From the results obtained, it was proposed that the stretching vibration of CO adsorbed on Cu^+ appearing at 2154 cm^{-1} corresponds to Cu sites located in the zeolite cavities, whereas the stretching vibration at 2135 cm^{-1} is proposed to be characteristic of Cu^+ sites located in

constrained environments, such as the 6Rs.[100] These results were further supported by DFT-based calculations of vibrational frequencies.[102]

Giordanino et al. employed FT-IR transmission spectroscopy of adsorbed CO to characterise a Cu-SSZ-13 zeolite pre-activated either in O_2 flow or in vacuum.[101] From the results obtained the authors observed the presence of several Cu species, including isolated Cu^+ ions able to form mono-, di- and tricarbonyl species, and monovalent Cu^+ and $[Cu^{2+}(OH)^-]^+$ species upon O_2 activation. As also seen by some of us,[100] at low CO coverage, monocarbonyl $Cu^+(CO)$ complexes were first formed, though different intensities were obtained for this feature depending on the activation treatment. To explain this discrepancy, the authors argued that only the strongest adsorption processes could be monitored in the experiments performed by Szanyi et al.,[100] as CO adsorption was performed at RT, so no differences could be observed on the spectra collected on annealed, oxidised or reduced samples. Increased CO coverage lead to the formation of dicarbonyl $Cu^+(CO)_2$ complexes, together with the evolution of a broad band around 2220 – 2235 cm^{-1}, assigned to Al^{3+}...CO adducts, resulting from the presence of extraframework Al species. At low to medium CO coverages, monocarbonyl complexes located in constrained environments, such as in 6Rs, were observed (2135 cm^{-1}), while at higher CO coverage, tricarbonyl complexes and OH...CO adducts on the Brønsted acid sites and the external silanol groups were formed. Interestingly, at the highest CO coverage a sharp peak at 2207 cm^{-1} emerged on the O_2 activated sample, attributed to Cu-OH...CO adducts, resulting from the presence of $[Cu^{2+}(OH)^-]^+$ complexes (vide infra).[101]

IR spectroscopy of adsorbed CO has also been used to characterize Fe species in Fe-SSZ-13.[103] The interaction of CO is weak with Fe ions in Fe-SSZ-13 zeolites, therefore IR spectroscopy can only be performed at low sample temperatures to study CO adsorption. IR

spectra collected at 100 K sample temperature over Fe-ZSM-5 exhibited a vibrational feature of adsorbed CO on Fe^{2+} ions only, while no adsorbed CO signal on Fe^{3+} sites were observed.[104] Gao et al. investigated the adsorption of CO on both fresh and hydrothermally aged (HT) Fe-SSZ-13 zeolites at 150 K sample temperatures.[103] The fresh sample (calcined at 773 K for 2h in vacuum) exhibited a number of IR bands characteristic of carbonyl species bound to Fe^{2+} (2194 cm^{-1}), Al^{3+}-bound CO (2220 cm^{-1}) and zeolitic OH-bound CO (2175 cm^{-1}). The thermal stabilities of these adsorbed CO were very low, the highest being the Fe^{2+}-adsorbed CO. After hydrothermal aging (1073 K for 16 h) the Fe-SSZ-13 sample displayed two new IR features upon CO exposure at 150 K at 2153 and 2138 cm^{-1}, in addition to those observed for the fresh samples. The weak absorption feature at 2153 cm^{-1} may be assigned to CO adsorbed onto finely dispersed FeO_x clusters formed during the high temperature hydrothermal aging, while the 2138 cm^{-1} band is attributed to CO adsorbed onto Fe^{2+} ions in the vicinity of some extraframework cations, most probably Al^{3+}.[103]

3.2.2.2. IR Spectroscopy of adsorbed N_2

N_2 has been increasingly used as a probe molecule because it is completely unreactive and highly specific as a very weak base. Even though N_2 is infrared inactive, a decrease in the symmetry of the molecule can lead to infrared activity of the N−N stretching mode when the molecule is within an anisotropic environment.[105] IR spectroscopy of adsorbed N_2 has been employed by Giordanino et al. to get further insight into the Cu species formed upon vacuum activation; whereas N_2 molecules interact with Cu^+ ions forming $Cu^+(N_2)$ adducts, the interaction with Cu^{2+} ions is too weak.[101] In agreement with results obtained using CO as a probe, the spectra displayed two different components upon N_2 adsorption, at 2293 and 2300 cm^{-1}, attributed to $Cu^+(N_2)$ complexes located in different environments. Additionally, the interaction

of N_2 with either the Brønsted sites or extra-framework Al species was also investigated, confirming the presence of small amount of EFAl species.[101]

3.2.2.3. IR Spectroscopy of adsorbed NO

IR spectroscopy of adsorbed NO is a commonly used method for zeolite characterisation, which provides information about Lewis acidity and redox properties of cationic sites. The coordination of NO to a cationic site leads to the formation of surface nitrosyl species, which absorb in a wide spectral range. As with CO, NO is commonly used as a probe molecule to investigate the oxidation state and location of Cu species on zeolites, since it is able to coordinate with both Cu^+ and Cu^{2+} ions; the use of NO as an IR probe has been recently reviewed.[96-98] Kwak et al. performed NO adsorption measurements on Cu-SSZ-13 zeolites with different ion exchange levels.[99] Before the measurement, the zeolite samples were annealed in vacuum at 400 ºC for 2h, so a part of the Cu^{2+} species were autoreduced to Cu^+ ions. Accordingly, vibrational features corresponding to NO molecules adsorbed on both Cu^{2+} (1948 and 1914 cm^{-1}) and Cu^+ (1810 and 1780 cm^{-1}) sites were seen in the spectra. Since more than one distinctive band was observed on each site (in line with the results obtained using CO), it was proposed that in Cu-SSZ-13, both Cu^{2+} and Cu^+ occupy two different cationic positions; i.e. inside the 6R and in the large zeolite cages.[99] Subsequent studies further confirmed the findings reported above.[100] Transmission FT-IR investigations on Cu-SSZ-13 samples submitted to different pre-treatments (i.e. annealed in vacuum, oxidised or else reduced with CO or H_2 and then annealed in vacuum) revealed that NO adsorbed on both Cu^+ and Cu^{2+} sites occupy positions in either the 6R and 8R, and that the $\upsilon_{N\text{-}O}$ peak position was sensitive to the location of the Cu ion in the CHA structure.[100] One of the key findings of this study was the identification of the origin of the IR absorption feature observed at ~2165 cm^{-1} on both the annealed and oxidized sample.

Measurements with ^{15}NO clearly showed that this feature belongs to an N-O stretching vibration whilst the peak position suggested that it corresponds to a positively charged species, most probably to NO^+. The evolution of the intensity of this band always paralleled that of the Cu^+-bound NO vibration on oxidized and annealed Cu-SSZ-13 samples, indicating that NO^+ species were produced by the reduction of Cu^{2+} sites by NO. NO^+ formation has been observed in other zeolites, in particular in ZSM-5, but primarily was associated with the reaction of $[NO^+][NO^{2-}]$ with protonic sites. As depicted in Figure 7, there seems to be a direct correlation between the amount of NO^+ and the amount of NO adsorbed onto Cu^+; as NO reduces Cu^{2+} to Cu^+, NO^+ forms and the thus produced Cu^+ ions can adsorb NO (intensity increase of the 1810 cm^{-1} band as the 2165 cm^{-1} band develops). Interestingly, co-adsorption of H_2O and NO on Cu-SSZ-13 resulted in the increase of the IR peak intensity of the NO species adsorbed onto Cu^{2+} ions in the 8R, and a concomitant decrease in the intensity if the IR band of adsorbed NO on the Cu^{2+} ions in the 6R,[100] in line with a prior study that showed how the reducibility of Cu^{2+} ions increased as they were pulled out from their most stable position (6R) into the large cage of the CHA structure, close to the 8R.[99] FT-IR spectra of NO adsorbed on pre-oxidised Cu-SSZ-13 with increasing ion exchange levels provided information about the variation of the population of the two distinct cation positions; while at low (~20%) ion exchange levels most of the Cu^{2+} ions are located in the thermodynamically most stable cationic position associated with the 6R, with increasing ion exchange levels the fraction of Cu^{2+} ions in the 8R sites increase, becoming dominant at the highest extent of exchange (~ 80 %).[106] Moreover, NO adsorption on these Cu-SSZ-13 samples revealed that Cu^{2+} ions in the 6R were very difficult to reduce, whereas Cu^{2+} ions in the 8R positions are readily reduced by NO. In agreement with mechanistic studies on

Cu-ZSM-5, the NO^+ ions formed in Cu-SSZ-13 zeolites by the reduction of Cu^{2+} to Cu^+ were proposed to be key intermediates in the overall NH_3-SCR reaction mechanism.[106, 107]

The effect of the activation treatment (i.e. either in O_2 flow or in vacuum) on the type and nature of Cu species was further investigated by Giordanino et al.[101] $Cu^+(NO)$ mononitrosyl complexes were detected at low NO coverage on the vacuum activated sample, while increasing coverage resulted in the formation of $Cu^+(NO)_2$ dinitrosyls. Both types of species were also detected on the O_2 activated sample, probably due to the pre-treatment, after desorption experiments had been carried out. Interestingly, the bands of mononitrosyl and dinitrosyl species exhibit a very similar shape and position to those observed on the vacuum activated sample, indicating that Cu^+ location and distribution is not affected by the activation treatment. Additionally, bands corresponding to $Cu^{2+}(NO)$ species were also seen in the spectra, with different contributions, possibly due to the location of Cu^{2+} ions at different cation positions. In line with the results obtained using CO as a probe, a band assigned to Cu-OH...NO adducts (1890 cm^{-1}) was detected, providing further support to the presence of $[Cu^{2+}(OH)^-]^+$ species in O_2 activated Cu-SSZ-13.[101]

NO has also been used as a molecular probe to characterize Fe^{2+} ions in both fresh and HTA Fe-SSZ-13 samples.[103] The IR spectra for the fresh catalyst recorded at room temperature after annealing at 773 K for 2 h were very similar to those reported for other Fe-exchanged zeolites,[108-113] showing the presence of mono-, di-, and tri-nitrosyl species associated with Fe^{2+} ions within the SSZ-13 structure (Figure 8). At low NO coverage, a vibrational feature characteristic of Fe^{2+}-bound mono-nitrosyl species developed at 1887 cm^{-1} with a shoulder at 1902 cm^{-1}, representing nitrosyl groups adsorbed to Fe^{2+} ions in two different coordination environments. Increasing NO coverage resulted in the appearance of new features at 1772 and

1833 cm^{-1}, representing N-O vibrations of Fe^{2+}-bound dinitrosyl species. Concomitantly, another IR band developed at 2158 cm^{-1}, attributed to NO^+ species. The intensities of all of these bands increased with increasing NO coverage, and eventually new bands of Fe^{2+}-bound tri-nitrosyls appeared at 1916, 1813 and 1801 cm^{-1}. As molecularly adsorbed NO in $Fe^{2+}(NO)_3$ species are weakly held, it could be completely removed by evacuation at room temperature. Dinitrosyl and mononitrosyl species were consecutively decomposed upon heating from 295 to 500 K, while NO^+ species were still present even after annealing at 500 K.[103]

IR spectroscopic studies using NO have also been performed to get further insight into the intermediate species formed during the SCR reaction. Ruggeri et al. recently performed an in situ DRIFTS study of NO_2, $NO+O_2$ and NO adsorption to investigate NO oxidation to NO_2,[114] previously proposed to be the rate-determining step for the SCR reaction (see section 4. Catalytic Chemistry and Mechanisms). Both NO^+ (2140 cm^{-1}) and nitrates (bidentate nitrates at 1590 and 1570 cm^{-1}, and bridging nitrates at 1620 cm^{-1}) were simultaneously detected upon NO_2 introduction, whereas nitrates appeared only after NO^+ when the catalyst was exposed to $NO+O_2$. Accordingly, nitrosonium cations (NO^+) were proposed as key intermediates, and two different mechanisms were anticipated for their formation from either NO_2 or $NO+O_2$, i.e. oxidation of NO on Cu^{2+} sites and NO_2 disproportionation. Notably, no NO^+ and nitrates were formed on a pre-reduced Cu-SSZ-13 sample when only NO was feed, providing evidence of the redox nature of NO oxidation to NO_2. According to the results obtained, and assuming that NO oxidation takes place on Cu dimers, a reaction mechanism was proposed.[114]

Formation of nitrates on Cu-SSZ-13 upon $NO+O_2$ or NO_2+O_2 adsorption has been recently reported by different groups. Xie et al. indicated the formation of monodentate (1504 cm^{-1}), bidentate (1573 and 1596 cm^{-1}) and bridging nitrates (1631 cm^{-1}) on a Cu-SSZ-13 zeolite

prepared by one-pot synthesis methods,[115] while different assignments were proposed by Ma et al.[116] At low temperatures (100 ºC), bands at 1574 and 1601 cm^{-1} were detected, attributed to bidentate and monodentate nitrates, respectively, together with a band at 1500 cm^{-1}, assigned to nitrite species. The intensity of these bands decreased with increasing temperatures (200 ºC), concurring with the appearance of a new feature at 1622 cm^{-1}, attributed to surface adsorbed NO_2.[116]

Additionally, DRIFT spectroscopy of adsorbed NO has been employed to gain information on the effects of hydrothermal ageing on Cu-SSZ-13 zeolites with different Cu loadings and Si/Al ratios.[117] In agreement with previous works, the spectra recorded for the fresh catalysts showed the presence of NO adsorbed on Cu^{2+} sites located in the CHA cages (1910 cm^{-1}), NO adsorbed on Cu^{2+} located on the 6R units (1948 cm^{-1}), and NO adsorbed on the Cu^{+} ions (1810 cm^{-1}), most likely formed during the catalyst pre-treatment. After ageing at 850 ºC, the peaks of NO adsorbed on Cu^{2+} sites decreased in intensity for the low and medium Cu-loaded samples, while for the high-loaded samples or else the samples with high Si/Al ratio these peaks were absent. Based on these findings, it was concluded that Cu^{2+} species located on the CHA cages are more prone to agglomerate during hydrothermal ageing, leading to the collapse of the zeolite structure. Thus, the hydrothermal stability of the catalyst decreases with increasing Cu loadings or with decreasing Al contents (i.e. as the relative number of framework Al atoms in the 6*R* decreases or the Cu content increases, more Cu^{2+} ions are likely to be coordinated in the CHA cage, wherein the aggregation of Cu species is favoured).[117]

3.2.2.4. IR Spectroscopy of adsorbed NH_3

Ammonia is probably one of the most frequently used probe molecules for the characterisation of acid properties of solid catalysts. It is small in size and a hard Lewis base, so can be strongly bonded to a wide variety of sites. Therefore, it cannot be considered as a very specific probe molecule and it may not always provide ideal properties for studies of surface acidity.[105] Nevertheless, the use of NH_3 as a probe is of special interest for the investigation of the SCR reaction, as it is employed as the NOx reducing agent. In particular, research efforts have been focused on the study of NH_3 adsorbed species and their reactivity under SCR conditions, essential to elucidate the role of the different species in NH_3 storage, as well as their contribution to NH_3 slip.

Zhu et al. employed for the first time DRIFT spectroscopy to investigate the type and nature of NH_3 adsorbed species on Cu-SSZ-13 (activated at 773 K for 1 h in flowing He).[118] After NH_3 adsorption at 373 K, the IR spectra displayed different features corresponding to two distinct NH_3 species; bands at 3352, 3182 and 1620 cm^{-1} were assigned to adsorbed NH_3 on Lewis acid sites (i.e. Cu ions), while features at 3262 and 1454 cm^{-1} were attributed to adsorbed NH_3 on Brønsted acid sites, present as a result of the incomplete ion exchange of the catalyst.[118] In zeolite materials, a Brønsted acid site corresponds to the proton used to charge balance –Al-O(H)-Si- species and where, upon adsorption, NH_3 becomes protonated forming NH_4^+ ions. A Lewis acid site, on the other hand, describes a coordinatively unsaturated electropositive species that can interact with a Lewis base i.e. molecular NH_3, to form a chemical bond via the lone pair onNH_3. A Lewis acid site can be extra-framework Al sites, or extra-framework cationic sites (including Cu-ion sites). In partial agreement, Lezcano-Gonzalez et al. combined FT-IR transmission spectroscopy of adsorbed NH_3 with DFT-based simulations, indicating the presence of at least three types of NH_3 adsorbed species on Cu-SSZ-13 samples with different ion

exchange levels, activated at 523 K under flowing O_2.[88] As seen in Figure 9, these included ammonium ions (1448 and 1393 cm^{-1}, $\delta(NH_4^+)_{as}$ and $\delta(NH_4^+)_s$, respectively), formed on the Brønsted acid sites, $[Cu(NH_3)_4]^{2+}$ complexes (1619 and 1278 cm^{-1}, $\delta(NH_3)_{as}$ and NH_3 wagging, respectively), resulting from NH_3 coordination with the Cu^{2+} Lewis sites, and NH_3 adsorbed on extra-framework Al (EFAl) species (1620 and 1324 cm^{-1}). Interestingly, the FTIR spectrum of the Cu-SSZ-13 sample with 100 % exchange, showed two intense bands of the bridging hydroxyl groups, at 3605 and 3585 cm^{-1}, comparable to those observed for the parent material, indicating that Brønsted acid sites remained in the sample despite complete Cu^{2+}-exchange. Additionally, a broad band centred at 3655 cm^{-1} was also present, previously attributed to the ν(OH) stretch of $[Cu^{2+}(OH)^-]^+$ complexes.[101] Accordingly, the authors indicated that some of the Cu^{2+} ions were also probably present in the form of monovalent complexes, thereby resulting in an incomplete reduction in the number of Brønsted acid sites.[88] In relation to this, it is worth noting that, recently, the formation of $[Cu^{2+}(OH)^-]^+$ species on Cu-SSZ-13 zeolite upon dehydration under O_2 flow has been confirmed by FT-IR spectroscopy, and explained according to two different mechanisms, depending whether only one or two framework Al sites were in close proximity.[76]

Following a similar approach, Giordanino et al. have also indicated the presence of several types of NH_3 species.[119] Besides to NH_4^+ ions formed on the Brønsted acid sites and NH_3 adsorbed on the Cu sites, it was shown that solvated NH_4^+ species were also present. Furthermore, in line with the results reported by Lezcano-Gonzalez et al.,[88] the authors observed that the intensity of the bands of the Brønsted acid sites were higher than expected and comparable to the parent H-form zeolite, pointing to the presence of monovalent Cu complexes, such as $[Cu^{2+}(OH)^-]^+$ species. On the basis of NH_3-temperature programmed desorption followed

by FT-IR, it was revealed that NH_3 bonded to Brønsted sites were more abundant at high temperatures (> 673 K), while at lower temperatures, both solvated NH_4^+ species and NH_3 bonded to Cu sites were more stable.[119]

3.2.2.5. In situ/in operando IR SCR studies

To investigate the reactivity of the NH_3 species formed on Cu-SSZ-13, Zhu et al. employed *in situ* DRIFTS (i.e. combined with simultaneous analysis of gas products by mass spectrometry) using gas feeds of NO_2, $NO+O_2$, and NO_2+O_2.[118] Importantly, at low temperatures, NH_3 species adsorbed on Lewis acid sites were more active than those adsorbed on Brønsted sites. The overall reaction rate increased with increasing reaction temperature, and was faster when using $NO+O_2$ or NO_2+O_2 that NO_2 alone. Moreover, the selectivity to N_2 was much higher when $NO+O_2$ or NO_2+O_2 mixtures were used.[118] In line with these findings, Lezcano-Gonzalez et al. performed in situ FT-IR transmission studies of the reaction of adsorbed NH_3 under standard SCR conditions, indicating that NH_4^+ ions formed on the Brønsted acid sites reacted very slowly in comparison to NH_3 coordinated to the Cu^{2+} ions.[88] From the results obtained, it was concluded that NH_4^+ ions barely contribute directly to the SCR process, and that Brønsted acid sites may not be indispensable, acting merely as NH_3 storage sites. Importantly, the results obtained on a Cu-SSZ-13 sample with 100 % exchange (i.e. prepared by successive ion exchanges) showed a substantial increase in the reaction rate of NH_4^+ species, suggesting that the availability/reactivity of NH_4^+ ions can be notably improved by submitting the SSZ-13 zeolite to repeated exchanges with Cu^{2+}.[88]

Ma et al. employed in situ DRIFTS to compare the reactive properties of Cu-SSZ-13 and Cu-SAPO-34.[116] Prior to the experiments, drilled cores of Cu-SSZ-13 and Cu-SAPO-34 washcoated on cordierite monoliths were aged at 750 ºC for 16 h in a nitrogen gas mixture with

14 % O_2, 5 % CO_2 and 5 % H_2O and the aged catalysts were scrapped from the monoliths to obtain powder samples. At low temperatures (220 ºC), DRIFTS spectra for the reaction of adsorbed NH_3 and NO, NO+O_2, NO_2 and NO+NO_2 showed the formation of nitrate species and NO_2. The catalytic reaction was greatly improved when NO and NO_2 were simultaneously introduced, whereas the presence of oxygen increased the reaction rate of the NH_4^+ ions. A similar reactivity was observed for Cu-SAPO-34, suggesting that the NH_3-SCR reaction might follow similar routes for both catalysts. When the reaction was carried out at higher temperatures (350 ºC) the reactivity of NH_4^+ ions followed the order NO_2>NO+O_2>NO on both Cu-SSZ-13 and Cu-SAPO-34. Nevertheless, NH_4^+ ions were consumed earlier on the SAPO-34, indicating a faster reaction rate, in agreement with the activity data.[116] Following the same approach, the effects of propene poisoning were also examined.[120] Additionally, coked samples were prepared at 350 ºC for 6 h using a gas mixture with 500 ppm C_3H_6 and 10 % O_2 in N_2. From the results obtained it was shown that, at low temperatures, competitive adsorption between NO_x and C_3H_6 contributed to the deactivation of Cu-SSZ-13, while NH_3 adsorption was not inhibited by the presence of propene or influenced by coke deposition. Conversely, at higher temperatures the deposition of coke was the main reason for catalyst deactivation.[120]

In situ DRIFTS experiments have been also conducted to investigate the inhibitory effect of NO_2 over one-pot-synthesized Cu-SSZ-13 zeolite.[115] Initially, the catalyst was only exposed to 1000 ppm NH_3/N_2 or 1000 ppm NO (NO_2) + 5% O_2 so as to identify the type of adsorbed species. Upon NH_3 adsorption, bands corresponding to NH_4^+ species and NH_3 coordinated to the Lewis acid sites were detected, whereas exposure to NO+O_2 or NO_2+O_2 lead to the formation of three types of nitrate species; i.e. monodentate, bidentate and bridging nitrates. Experiments under standard SCR conditions showed the formation of adsorbed NH_3 species on both Lewis

and Brønsted acid sites, as well as a small amount of NH_4NO_3. Conversely, under fast SCR conditions the formation of NH_4NO_3 species was favoured. Since NH_4NO_3 species could block the zeolite pores and deactivate the active sites, the authors concluded that the greater amount of NH_4NO_3 deposited was the main reason for the inhibitory effect of NO_2 on the NH_3-SCR reaction in the low temperature range.[115]

Mechanistic DRIFTS studies on heterobimetallic (La, Fe, Sc and In) Cu-SSZ-13 zeolites have also been carried out to elucidate the origin of the exceptional performance of these materials at low reaction temperatures.[121] From the results obtained it was suggested to be related the formation of a higher concentration of NO^+ species, which possibly play an important role in the fast SCR reaction. Presumably, the heterobimetallic core favours the disproportionation reaction between NO and NO_2 to form and stabilise NO^+ and NO_2^-.[121]

In operando DRIFTS has also been employed to investigate the interaction of $NO+O_2$ and NH_3 over a $Fe_{1.32}$/Cu-SSZ-13 catalyst.[122] It was shown that cis-$N_2O_2^{2-}$, NO^{3-} and NO^+ species, generated from $NO+O_2$ adsorption, were readily reduced to N_2 by both Lewis acid site-adsorbed NH_3 and Brønsted acid site-adsorbed NH_3, evidencing that both NO^+ and NO_3^- are key intermediates in the NH_3-SCR reaction.[122]

3.2.2.6. IR spectroscopy of perturbed framework vibrations

In addition to the identification of adsorbed molecules on different cationic sites in Cu-SSZ-13 zeolites, IR spectroscopy has also been used to investigate the influence of metal ions in ion exchange positions on the T-O-T vibrations of the zeolite framework.[75, 99] Extensive IR spectroscopy studies on the "perturbed" asymmetric T-O-T framework vibrations have been conducted mostly on the MFI structure.[123-131] These investigations have shown that certain T-O-

T vibrational modes (IR features in the 800-1000 cm^{-1} spectral region representing asymmetric internal T-O-T vibrations of the zeolite framework) are very sensitive to both the oxidation state of the Cu ions, as well as to the adsorbates bound to these ions.[123-131] The results of an in situ DRIFTS study indicated that there were two perturbed T-O-T vibrations in Cu-SSZ-13, and that the intensity ratio of these two IR features varied with Cu ion exchange level.[99] At low Cu ion exchange level (~20 %) only one band was observed at ~ 900 cm^{-1}, but with increasing Cu content another IR band developed at ~945 cm^{-1}. These two bands were assigned to the perturbed asymmetric T-O-T vibrations of the CHA structure in the vicinity of two distinct Cu^{2+} ion locations: Cu^{2+} in the 6R (~900 cm^{-1}), and Cu^{2+} in the 8R. Cu^{2+} ions in these two distinct ion exchange positions exhibited different propensity toward reduction: Cu^{2+} ions in both positions were reduced to Cu^{+} in H_2, but Cu^{2+} in the 8R were reduced first followed by the reduction of Cu^{2+} ions in the 6R.[99] Kwak et al., have shown that in a CO/He flow all the Cu^{2+} ions in the 8R were reduced to Cu^{+}, while Cu^{2+} ions in the 6R were completely resistant to reduction under the experimental conditions applied.[75] The combined DRIFTS/XANES study of Kwak et al., has also revealed that the interaction between the Cu ions and the zeolite framework is influenced by the adsorbates bound to the Cu ions. For example, in the presence of adsorbed water in the zeolite channels (when Cu^{2+} is present in a hexa-aqua complex) the interaction between the cation and the framework is weak, thus the perturbed T-O-T vibrations are almost completely absent. Furthermore, when CO is adsorbed onto Cu^{+} ions, the strength of cation/framework interaction is dependent upon the number of CO molecules bound to the copper ion, and can be followed by both the position and the intensity of the perturbed asymmetric T-O-T vibrational features of the CHA framework (Figure 10). The variations in the IR spectra of perturbed T-O-T vibrational features clearly indicated that Cu ions in the CHA framework are highly mobile, and

their exact positions are determined by the ion exchange level, and, most importantly, their interaction with molecules present in their environment.[75] Under practical operating conditions, in the presence of strongly interacting adsorbates (e.g., H_2O, NH_3, NO_x, CO) cations most likely reside in positions different from their idealized cationic sites in the adsorbate-free CHA framework.

3.3. Electron Paramagnetic Resonance (EPR) Spectroscopy

Electron paramagnetic resonance (EPR) spectroscopy is a powerful tool for the characterisation of transition metal-containing zeolites, especially due to its very high sensitivity as compared to other spectroscopic techniques. It provides valuable information about the oxidation state and local environment of paramagnetic metal ions, allowing discriminating between different geometries and types of ligands.

EPR spectroscopy has been successfully used in the characterisation of Cu-containing zeolites, especially for the determination of the oxidation state of the Cu species, its symmetry and coordination number, or else its location within the zeolite structure. Moreover, a number of studies have been devoted to the investigation of Cu self-reduction, known to occur as a result of the catalyst pre-treatment under inert or high vacuum conditions. More information about the technique and its application to the study of Cu-containing zeolites can be found elsewhere.[132]

Gao et al. employed EPR spectroscopy to characterise hydrated Cu-SSZ-13 zeolite samples with different Cu loadings.[133] Spectra recorded at room temperature showed all Cu species to be present as EPR active Cu^{2+} ions, as confirmed by the gradual increase in the signal intensity with increasing Cu contents. Note that both Cu^{+} ions and Cu^{2+} dimers are EPR silent species. Two distinct features were observed at high field, at 3334 and 3407 G, with the latter dominating the spectrum at low Cu loadings and becoming a shoulder at high loadings.

Hyperfine features at low field (i.e. hyperfine interaction between the unpaired electron and the nuclear spin of Cu (I=3/2)) were however, not well resolved, possibly due to both Cu^{2+} mobility and strong dipolar interactions between Cu^{2+} ions. Additionally, experiments were also conducted at 155 K. As depicted in Figure 11, the recorded spectra exhibited a single feature at high field, and a better resolved single hyperfine structure at low field. The extracted g-value and hyperfine coupling constant ($g_{\|}$ = 2.394 and $A_{\|}$ = 131 G) indicated the presence of Cu^{2+} ions in octahedral coordination. Again, a linear relationship between Cu content and signal intensity was also found.[133]

In addition, Cu–Cu distance estimations based on line broadening of EPR spectra, attributed to distance-dependent dipole-dipole interactions between Cu^{2+} ions, were also carried out. At low Cu loadings, Cu-Cu distances were above 20 Å, suggesting one Cu^{2+} ion within one hexagonal unit cell, possibly located within the large CHA cages coordinated to lattice oxygen atoms of the 6Rs. At higher Cu contents, the estimated Cu-Cu distances substantially decreased, increasing the probabilities of Cu^{2+} ions to be located within the same unit cell and thereby, suggesting the presence of some Cu ions occupying positions in the large CHA cages and close to the 8Rs.[133]

With the aim to further characterise the EPR active Cu^{2+} species, Giordanino et al. performed EPR measurements on hydrated and O_2 activated Cu-SSZ-13 samples, recording the spectra at room temperature.[101] The results obtained on the fully hydrated sample were in complete agreement with those reported by Gao et al., showing all Cu to be EPR active. Again, the intensity of the EPR signal correlated with the Cu content, further confirming that all Cu species are present as Cu^{2+} ions. Interestingly, both isotropic and anisotropic features were observed in the spectrum, indicating that part of the Cu species present have full rotational

freedom. In contrast, only anisotropic Cu was observed after O_2 activation, attributed to a stronger interaction between Cu and the CHA framework once the hydration shell of Cu is lost.[101]

Later, Gao et al. employed EPR spectroscopy to investigate hydrated Cu-SSZ-13 samples with very low Cu loadings, so as to avoid dipolar interactions between Cu^{2+} ions.[134] Hyperfine features showed more than one Cu^{2+} species, suggesting that part of the Cu^{2+} ions are interacting with the framework. While for the spectra recorded at 120 K line-broadening was not observed, the spectra acquired from room temperature to 200 ºC showed the Cu^{2+} ions to be highly mobile, only becoming immobile again upon extensive dehydration (at 250 ºC), in line with the results obtained by Giordanino et al.[101] The lack of hyperfine structures and the loss of high-field signal between 100 and 200 ºC were attributed to dipolar interactions between Cu^{2+} ions, while the formation of EPR silent species, such as Cu^{+}, was ruled out. To further support this, complementary FT-IR experiments of adsorbed NO were carried out, evidencing that Cu^{+} species were not formed after dehydration at 150 ºC.[134]

Very recently, in situ EPR studies have been performed during different dehydration and rehydration treatments, providing quantitative data about the Cu species present in Cu-SSZ-13.[135] It was reported that after dehydration, only 25 % of the Cu present is EPR active, corresponding to isolated Cu^{2+} species in the 6R rings balanced by two framework Al atoms (18 %), five-coordinated Cu^{2+} sites (4 %), and Cu^{2+} in noncrystalline Al sites (3 %). Based on the signal recovery after different treatments, EPR silent species were also tentatively assigned; i.e. Cu^{2+}-O-Cu^{2+} dimers (12 %), $[Cu^{2+}(OH)^{-}]^{+}$ species (50 %), that easily auto-reduce under He, and noncrystalline polynuclear copper oxide clusters and subnanoparticles (13 %). It was argued that in $[Cu^{2+}(OH)^{-}]^{+}$ complexes, Cu^{2+} is in a planar coordination and thus, EPR silent due to pseudo

Jahn-Teller effect. After water exposure, Cu^{2+} acquires a tetragonal environment, then becoming EPR active. Likewise, dimeric species easily undergo hydrolysis and become EPR active when exposed to water, forming two $[Cu^{2+}(OH)^{-}]^{+}$ monomers that successively recover the hydration shell.[135]

Alternately, EPR spectroscopy has been also employed by several groups to characterise the Cu species present on Cu-SSZ-13, investigating the type and nature of Cu ions in one-pot synthesised Cu-SSZ-13,[136] the influence of heteroatom incorporation [121] or else effect of hydrothermal deactivation,[92, 117, 137] amongst others.

3.4. Solid-State Nuclear Magnetic Resonance (NMR) Spectroscopy

Solid-state NMR is a short-range, element specific spectroscopy that provides information about the local environment around a particular element. Though being less sensitive than other spectroscopic techniques, it has been widely used for the structural and dynamic characterisation of zeolites, especially for the investigation of the local structure of framework and extra-framework atoms, surface acid sites, interaction and dynamics of adsorbed species (e.g. organic structure directing agents), or else location and mobility of exchangeable cations. For further information on the application of Solid-State NMR to the characterisation of zeolites, see.[138]

In the particular case of Cu-containing zeolites, solid-state NMR has been mostly applied to study the distribution of Al species within the zeolite framework, namely by ^{29}Si and ^{27}Al Magic Angle Spinning (MAS) NMR experiments. Al distribution may affect the structure and location of the Cu species and thus, their catalytic activity. Additionally, ^{27}Al MAS NMR has been used to investigate the influence of hydrothermal and chemical deactivation, which can lead

to the extraction of tetrahedrally-coordinated framework Al atoms and thus, the formation of extra-framework species. The different Al species present can be readily detected by ^{27}Al MAS NMR. It is worth to note however, that even though the isotropic chemical shift of Al offers information about the coordination, residual second-order quadrupolar broadening may result in a spectrum with not well-resolved resonances shifted with respect to their isotropic chemical shift. In this case, the MQMAS experiment can be used. Also importantly, it has to be considered that the presence of paramagnetic Cu species may also lead to a lower spectral resolution due to paramagnetic line broadening.

To date, several studies employing ^{27}Al MAS NMR spectroscopy for the investigation of hydrothermal and chemical deactivation of Cu-SSZ-13 zeolite have been published, and the main observations can be summarised as follows.[92, 139, 140] Framework dealumination takes place as a result of hydrothermal ageing, as seen by the pronounced decrease in the intensity of the signal of tetrahedral Al atoms (c.a. 50-60 ppm).[92, 139-141] However, no new peaks of extra-framework Al species, with octahedral coordination (c.a. 0-10 ppm), are detected, possibly due to the interaction between paramagnetic Cu and octahedrally-coordinated Al species.[92, 139] While no significant framework dealumination is observed after chemical deactivation by Zn, Pt or Ca introduction, a partial disruption of the zeolite framework occurs upon P poisoning; i.e. a significant decrease in the peak of tetrahedral Al is observed, concurring with the appearance of a broad resonance attributed to octahedral Al interacting with P.[142] The effects of P poisoning have been also complementary studied by ^{31}P MAS NMR spectroscopy, aiming to identify the type and nature of the species formed. While no $AlPO_4$ species are detected, P species with different degrees of polymerization are observed.[142] Additionally, ^{27}Al MAS NMR spectroscopy has been also employed to characterise Cu-SSZ-13 samples prepared by different methods (i.e.

conventional wet ion exchange and chemical vapour deposition), showing that no framework dealumination takes place as a result of the preparation method.[143]

^{15}N MAS NMR experiments have been also conducted to investigate the interaction of NO with Cu-SSZ-13 zeolite, specifically to obtain information on the nature and structure of Cu^{+}-NO^{+} complexes. Spectra recorded (Figure 12) using different spinning rates showed the presence of a signal centred at 399.7 ppm, assigned to Cu^{+}-bound NO^{-} as neither adsorbed NO nor Cu^{2+}-bonded NO_x are expected to be detected due to paramagnetic line broadening. Interestingly, the different intensity observed for the spinning side bands in each spectrum suggested an anisotropic environment for the nitrogen atom. Accordingly, the sideband pattern was fitted, determining the magnitude of the shielding anisotropy (δ = -230.2 ppm) and the asymmetry parameter (η = 0.15). As the observed asymmetry parameter was non-zero, it was concluded that there are no axial symmetry and hence, that the Cu-N-O atoms are not co-linear.

3.5. Mössbauer spectroscopy

Variable temperature ^{57}Fe-Mössbauer spectroscopy is ideally suited to investigate the nature of Fe species in the fresh and HTA (high temperature aged) Fe-SSZ-13 catalysts. Spectra collected from hydrated samples at both ambient and liquid nitrogen temperatures allowed the identification of iron species in different oxidation states (+2 and +3) and coordination environments.[103] The Mössbauer spectrum obtained from the fully hydrated fresh sample at room temperature suggested the presence of two types of Fe^{3+} species: monoferric $[Fe(OH)_2]^{+}$ and diferric-oxo $[HO\text{-}Fe\text{-}O\text{-}Fe\text{-}OH]^{2+}$ complexes. Acquisition of Mössbauer spectra at 77 K was essential to distinguish Fe species in different magnetic states and to identify Fe species that were Mössbauer silent at ambient temperature. In addition to the two Fe^{3+} species observed at ambient temperature the spectrum recorded at 77 K revealed the presence of two other Fe

species: Fe^{2+} and a minor Fe^{3+} in FeO_x clusters. The only detectable Fe species in the HTA Fe-SSZ-13 were also in the +3 oxidation state. In the spectrum recorded at 77 K (Figure 13) three different Fe species were identified, two representing Fe^{3+} and one Fe^{2+} ions. The somewhat different Mössbauer parameters of the Fe^{3+} species in the spectra of the HTA sample suggest that the environment around these Fe^{3+} ions had changed during the aging process; some of the Al^{3+} ions that were removed from the zeolite framework got included into the FeO_x clusters.[103]

3.6. Temperature-programmed techniques

3.6.1. Ammonia temperature-programmed desorption (NH_3-TPD)

Ammonia temperature-programmed desorption (NH_3-TPD) is one of the most extensively used methods for measuring the acidity of zeolites, providing information on the number of acid sites (i.e. Lewis or Brønsted) and the acid strength distribution.[144, 145] Thermal desorption of pre-adsorbed NH_3 results in a profile with different desorption peaks; while the temperature of a TPD peak is related to the acid strength of the adsorption sites, the peak areas can be correlated with the concentration of acid sites. As TPD peaks may overlap due to the simultaneous desorption of NH_3 from different sites, the technique can only be used to discriminate different acid strengths in an approximate way, and certainly limiting its applicability.[145] Furthermore, since TPD is unable to determine the origin of the adsorbed NH_3, it is often necessary to combine it with an *in situ* spectroscopy technique such as FTIR.[145]

The characteristic NH_3-TPD profile of Cu-SSZ-13 zeolite has three desorption peaks, designated as low, intermediate and high-temperature peaks, and corresponding to acid sites with different acid strength.[88] The low-temperature (LT) desorption peak, observed at c.a. 180 ºC, corresponds to weakly bound NH_3,[146] and has been previously assigned to either NH_3 molecules solvating the NH_4^+ ions (e.g., as $N_2H_7^+$ dimers) or to NH_3 desorbed from Lewis sites;[147] however,

its identification is still a matter of controversy. The high-temperature (HT) desorption peak, centred at 480 ºC, is considered to be due to strongly bound NH_3, arising from protonated NH_3 formed over the Brønsted acid sites,[146] whereas the intermediate-temperature peak, at 320 ºC, has been attributed to NH_3 adsorbed over the Cu^{2+} sites.[88] However, a few recent studies suggested acid strengths of certain Lewis acid sites to be same as Brønsted ones, therefore, the HT desorption peak may have contributions from strong Lewis acidity. [148-150]

NH_3-TPD performed in He and followed by FTIR allowed to identify the different desorption sites and to study the thermal stability of the NH_3 species adsorbed on the Cu-SSZ-13 catalyst.[119] The results obtained indicated the presence of NH_3 bonded to copper sites, protonated NH_3, formed on the Brønsted acid sites, and solvated NH_4^+ ions. While at 500 ºC NH_3 bonded to copper sites was completely desorbed, protonated NH_3 species were still present (Figure 14), suggesting a higher thermal stability for NH_4^+ ions. In addition, it was found that solvated NH_4^+ ions (i.e. $NH_4^+.nNH_3$ associations) were more stable at T < 400 ºC; desorption of solvating NH_3 molecules lead to non-solvated NH_4^+ ions, which further decomposed at temperatures above 400 ºC. [119]Additionally, NH_3-TPD has been applied in a number of studies for the characterization of Cu-SSZ-13 zeolite, so as to provide information about the effect of hydrothermal ageing or chemical deactivation on the zeolite NH_3 adsorption capacity.[120, 142, 151]

3.6.2. Hydrogen temperature-programmed reduction (H_2-TPR)

Hydrogen temperature-programmed reduction (H_2-TPR) is a useful tool for the determination of the mean oxidation state of the catalyst after reduction from the total amount of hydrogen consumed during the reduction process. Nevertheless, careful attention must be paid to the experimental conditions, since it can largely influence the results obtained.

As shown in Figure 15, the H_2-TPR profile of a low Cu-loaded (20 %) Cu-SSZ-13 zeolite exhibits one H_2 consumption peak at 340 ºC, while higher Cu-loaded samples (40 to 100 %) show an additional peak at lower temperatures (c.a. 230 ºC) that increases with increasing Cu loadings.[99] Conversely, the high-temperature peak remains unchanged at Cu ion exchange levels above 40 %, due to the presence of two Cu^{2+} species with different reducibility. The less reducible Cu^{2+} species have a stronger electrostatic interaction with the zeolite framework, highly coordinated with lattice oxygens, and are probably located inside the 6R or else placed within or close to the face of 6R. Once these sites are saturated, Cu^{2+} ions occupy cationic positions inside the large zeolite cages, and most likely are easier to reduce.[99]

4. Catalytic Chemistry and Mechanisms

The chemistry involved in NH_3-SCR is rather complicated. Not only are the elementary reaction steps, especially the ones that are rate-limiting, not fully understood, even the global pathways are complex enough that an extensive reaction network is generally required for a detailed description [5]. The mechanism for SCR over Cu/Fe ion exchanged zeolite catalysts is still widely debated. The key points of disagreement are the following:[152] (1) Whether the catalytically relevant Cu/Fe species are monomeric or dimeric (even, perhaps very small oligomeric clusters); (2) Whether NO_2 plays a significant role in the mechanism. While some researchers suggest it is important and its formation could even be the rate-limiting step,[5] others argue against this;[8, 153-155] (3) Whether Cu^{+}/Fe^{2+} plays an important role in standard NH_3-SCR. If so Cu^{2+}/Cu^{+} (Fe^{3+}/Fe^{2+}) redox cycling is important, otherwise it is likely not. (4) Whether Cu- and Fe-CHA are dual functional in SCR; that is, whether both Cu/Fe ion sites and Brønsted acid sites collectively provide the catalytic functionality. Note that it is much easier to propose a seemingly reasonable mechanism than to prove its rigidity. For the latter, a plausible one must be

consistent with reaction kinetics acquired without artifacts (mass and/or heat transfer limitations, etc.) and must be consistent with operando spectroscopic evidences. Perhaps equally challenging is to distinguish a possible reaction pathway from a dominant reaction pathway. For the various spectroscopic methods that can be used *in situ/in operando* for NH_3-SCR, none of them is without limitations. For example, diffuse reflectance infrared Fourier transform spectroscopy (DRIFTS) is widely available for in situ NH_3-SCR studies. However, this technique suffers from the fact that the spectra acquired are dominated by strongly bound species (NH_3, NH_4^+, nitrates) while the short-lived, potentially more important species (NO_x, nitrites) in elucidating a reaction mechanism, are often not detected and quantified. Therefore, DRIFTS may be used to identify certain reaction pathways, but it is often incapable of ruling out others. As another example, X-ray absorption near edge structure (XANES) provides powerful means of identifying Cu^{2+}/Cu^+ under standard SCR conditions. However quantification cannot be done without ambiguity because of the difficulty in defining "ideal" reference spectra for the Cu-ligand/adsorbate complexes under reaction conditions.

In view the complexities described above, most relevant catalytic chemistry for SCR, namely NO oxidation, NH_3 oxidation, and standard, fast and NO_2-SCR reactions will be presented individually in this section. Focus will be given on CHA-based catalysts. However it is not possible and not appropriate to isolate CHA-based catalysts from the huge body of literature on zeolite-based SCR catalysts. Key discoveries made on other zeolite-based SCR catalysts will also be included when needed. With regard to the disagreements in literature mentioned above, we intend to describe rather than judge different views unless our own studies provide strong evidence in favor of certain arguments.

4.1. NO oxidation

In the confined internal space provided by CHA cages, there exists a finite probability for NO oxidation ($2NO + O_2 = 2NO_2$) without the existence of Cu/Fe ions. To study the contribution from Cu/Fe ion sites, this "background" reaction should be considered and NO_2 formed via this route should be subtracted. By doing so, Gao et al. discovered that for Cu-SSZ-13 catalysts at Si/Al = 6, NO oxidation activity in the presence of H_2O is essentially zero below ~ 400 °C at Cu/Al ≤ 0.29 (Figure 16).[152] Similarly, Verma et al. also reported that under dry reaction conditions and at 270 °C, NO oxidation activity is absent at Cu/Al < 0.2 in their samples (Si/Al = 4.5) [95]. These findings lead to the following conclusions: (1) Cu-SSZ-13 samples with relatively low Cu/Al ratios are dominated with isolated Cu^{2+} ions, and (2) isolated Cu^{2+} ions are incapable of catalyzing NO oxidation to NO_2. These conclusions receive support from theoretical calculations that isolated Cu^{2+} in the face of the 6 ring is incapable of activating O_2.[95] Obviously, Cu moieties that are active for this reaction must be the ones that activate O_2: isolated Cu^{+}, Cu_xO_y oligomers (including Cu-dimers), or Cu_xO_y particles. In situ XANES measurements by Verma et al. appear to allow isolated Cu^{+} to be ruled out and leave Cu_xO_y oligomers the likely species. *Ex situ* EPR measurements by Gao et al. on freshly prepared Cu-SSZ-13 samples (Si/Al = 6) in a hydrated state reveal that essentially all Cu^{2+} ions (up to Cu/Al = 0.45) are detectable indicating that they are all isolated (Cu_xO_y oligomers are EPR silent).[53] This indicates that under NO oxidation reaction conditions, isolated Cu^{2+} ions can oligomerize to generate the active sites. In light of the fact that at high Cu loadings large amounts of isolated Cu^{2+} ions stay as $[Cu(OH)]^{+}$,[156] one plausible reaction that accounts for the generation of such active sites is shown below:

$$[Cu(OH)^{+} + [Cu(OH)^{+} \rightleftharpoons [Cu - O - Cu]^{2+} + H_2O \quad (3)$$

Although it is not clear at present whether or not a $[Cu-O-Cu]^{2+}$ species is the oligomeric moiety that presents in highly Cu-loaded Cu-SSZ-13 (double bridged μ-oxo and μ-hydroxo Cu-dimers, for example, are also the obvious candidates),[94] the important message here is that in order to oxidize NO to gaseous NO_2, Cu-moieties with extra lattice oxygen (ELO) are required. Still using $[Cu-O-Cu]^{2+}$ as a model active center, the reaction pathways can be written as the following, according to a Mars van-Krevelen (redox) type of mechanism:

$$[Cu^{II}-O-Cu^{II}]^{2+} + NO = [Cu^{I} - \quad - Cu^{I}]^{2+} + NO_2 \qquad (4)$$

$$2[Cu^{I} - \quad - Cu^{I}]^{2+} + O_2 = 2[Cu^{II}-O-Cu^{II}]^{2+} \qquad (5)$$

Another key message is a dynamic view of the Cu-ion centers under reaction conditions (as will be shown below, this also applies to other SCR-related reactions). For example, reaction (3) should be viewed as a reversible process such that at ambient conditions oligomeric species can hydrolyze to generate isolated ions while at elevated temperatures isolated ions can combine to generate active sites for certain reactions (e.g., NO oxidation). In this sense, one has to realize and be very cautious in correlating reaction kinetics and ex situ characterizations.

Figure 17 presents NO oxidation rates (normalized with sample weight, the same as Figure 16) as a function of temperature on a Fe-SSZ-13 catalyst (Si/Al =12, Fe/Al = 0.2) under both 'dry' and 'wet' reactions.[65] A direct comparison between Figures. 16 and 17 immediately reveals that Fe-SSZ-13 is substantially more active even than the highest Cu-loaded Cu-SSZ-13. In the absence of H_2O, this sample is even more active. Mössbauer spectroscopic measurements reveal that even at ambient hydrated conditions, this sample contains ~ 40 % dimeric Fe sites [65]. Following a similar argument shown above that monomers are incapable of catalyzing this reaction, one can conclude that dimeric Fe sites are the active centers for NO oxidation and in the absence of H_2O, density of such sites increases via reactions similar to that shown in (3).

However, the inhibition role for H_2O does not appear to be the destruction of active sites alone as suggested by Sjövall et al.,[149] competitive occupation with the reactants for the same sites should be considered as another cause. Indeed, according to a detailed kinetic study by Metkar et al., although H_2O greatly inhibits NO oxidation activities for both Cu- and Fe-zeolites, it does not alter parameters of their power law kinetic model shown below:[157]

$$R_{NO_{oxi}} = k_f \frac{[NO]^a[O_2]^b}{[NO_2]^c} \quad (6)$$

This study also reveals stronger inhibition from NO_2 for Cu-CHA ($c \approx 1.0$) than for Fe-ZSM-5 ($c \approx 0.5$) thus providing one explanation why Fe/zeolites are more active in NO oxidation.

4.2. NH_3 oxidation

NH_3 oxidation to N_2 ($4NH_3 + 3O_2 = 2N_2 + 6H_2O$) is referred to as "non-selective NH_3 oxidation" in standard NH_3-SCR as a major side reaction. The same chemistry, when, for example NH_3 slip elimination is concerned, is termed "selective catalytic oxidation (SCO)" instead [149, 158-163]. While performance type of studies are abundant, mechanistic studies for this reaction are surprisingly scarce.[158, 162] Ramis et al. used FTIR to investigate NH_3 adsorption and transformation on V_2O_5-based and CuO/TiO_2 catalysts.[158] The detection of N_2H_4 (in the absence of NO and O_2) allowed them to propose the following mechanism for N_2 formation:

$$NH_3(ads) = NH_2(ads) + H^+ + e \quad (7)$$

$$2NH_2(ads) = N_2H_4(ads) \quad (8)$$

$$N_2H_4(ads) = N_2 + 4H^+ + 4e \quad (9)$$

Such a mechanism is at least to some extent speculative since the detection of N_2H_4 was performed without the presence of O_2. Indeed, Amblard et al., when using DRIFTS to study surface vibrations of NH_3 and its derivatives on a Ni/Al_2O_3 catalyst in the presence of O_2, failed

to observe any spectroscopic similarity between NH_3/O_2 and N_2H_4.[164] Instead, they suggested a SCR-type of reaction mechanism involving two steps:

$$4NH_3 + 5O_2 = 4NO + 6H_2O \quad (10)$$

$$4NH_3 + 4NO + O_2 = 4N_2 + 6H_2O \text{ (Standard SCR)} \quad (11)$$

For zeolite-based catalysts (i.e., Fe-ZSM-5), Qi et al. were able to detect NO adsorbed on Fe sites via FTIR under NH_3 oxidation conditions.[162] They, therefore, also suggested the two-step mechanism. It should be noted that these proposals should not be judged as conclusive due to the intrinsic limitations of using FTIR to determine reaction mechanisms: a key reaction intermediate may very well be below the detection limit and that a detectable species may very well be a spectator. For Fe-zeolite catalysts, the correlation between N_2 selectivity for the SCO reaction and activity for the SCR reaction found by Yang and coworkers, i.e., catalysts display higher SCR activity also display higher N_2 selectivity in SCO, seems to better justify a two-step mechanism.[161, 162] In spite of uncertainty in the detailed reaction mechanism, however, a key elementary step must be hydrogen abstraction from adsorbed NH_3 (equation 7) and a high N–H bond energy for NH_3 (~390 kJ/mol) makes this step potentially a rate-limiting one.

To probe the nature of the Cu active centers, Gao et al. utilized a series of Cu-SSZ-13 samples with Si/Al = 6 and varying Cu/Al ratios (~0.11 to 0.45) to study NH_3 oxidation in the presence of ~2.5% H_2O in the feed.[53] This initial study substantiated three key points worth noting: (1) NH_3 oxidation rates increase with increasing Cu loading; (2) two kinetic regimes, separated at a common temperature of ~250 °C, are found; (3) apparent activation energies in the lower-temperature regime are ~130 kJ/mol and those in the higher-temperature regime are ~60 kJ/mol. From these experimental findings, it appears that the reaction rate limiting steps do not vary dramatically as a function of Cu loading, but they certainly do as a function of temperature.

In a subsequent study, the authors utilized samples with a wider range of Cu/Al ratios to further probe structure/function relationships. Figure 18 presents normalized rates (mol NH_3 g^{-1} s^{-1}) as a function of temperature in the differential regime and Figure 19 displays detailed reaction rate vs. Cu loading correlations at selected temperatures. As displayed in Figure 19(b), reaction rates vary linearly with Cu loading at ~ 350 °C and above. This linear behavior indicates fulfillment of the Koros–Nowak criterion [165, 166] so that mass and heat transfer limitations are ruled out; moreover, this strongly suggests that the catalytically active centers are isolated Cu-ion monomers. This follows since at such high temperatures and, especially for samples with relatively low Cu loadings, the presence of catalytic centers other than Cu-ion monomers is highly unlikely. Rather dramatically, however, at ~300 °C and below, reaction rates vary linearly only with the *square* of Cu loading.[152] While in a fully hydrated form at ambient conditions all Cu^{2+} ions in these samples are EPR detectable (including the highest Cu-loaded sample at Cu/Al = 0.45) indicating that they stay as isolated Cu^{2+} ion monomers,[53] under NH_3 oxidation conditions at relatively low temperatures, it appears that dimeric Cu centers that form under reaction conditions are the actual active centers.

Such transformation of Cu ion centers is not unexpected. Even at relatively low Cu loadings, Cu^{2+} ions should not be deemed as "naked" (i.e., Cu^{2+} ions coordinate only with lattice oxygen but not other extra-framework ligands) under low-temperature NH_3 oxidation conditions. H_2O and NH_3 storage by the CHA cages effectively creates a basic environment such that $[Cu(OH)]^+$ formation becomes highly likely:

$$NH_3 + H_2O \rightleftharpoons NH_4^+ + OH^- \quad (12)$$

$$Cu^{2+} + OH^- = [Cu(OH)]^+ \quad (13)$$

Furthermore, complexes of Cu^{2+} ions with NH_3, for example $[Cu^{II}(NH_3)_4]^{2+}$, $[Cu^{I}(NH_3)_2]^{+}$ and $[Cu(OH)(NH_3)_x]^{+}$, are also expected to form.[72, 88, 119] In essence, formation of such complexes weakens Cu-framework interactions and enhances Cu ion mobility. A reasonable speculation based on the kinetic results is that dimeric Cu-ion centers form from these mobile monomers via dehydration, condensation or coupling in the presence of O_2. Possible reactions can be written as follows:

$$2[Cu(OH)(NH_3)_x]^+ \rightleftharpoons [(NH_3)_x Cu - O - Cu(NH_3)_x]^{2+} + H_2O \quad (14)$$

$$2[Cu^I(NH_3)_2]^+ + O_2 \rightleftharpoons [(NH_3)_2 Cu^{II} - (\mu - O_2) - Cu^{II}(NH_3)_2]^{2+} \quad (15)$$

It should be emphasized that the existence of such Cu-dimer complexes has not been confirmed spectroscopically. However, no spectroscopic method is more sensitive to the dynamitic transformations of active centers than reactants themselves; and reaction kinetics are only consistence with their existence. Yet, another piece of indirect evidence comes from the dramatic change in reaction rate dependence on Cu loading with temperature (Figure 19). This is rationalized by the fact that at high temperatures of ~ 350 °C and above these Cu-dimer complexes become unstable (by losing extra-framework ligands) and split to Cu ion monomers. In this case, Cu ion monomers become the catalytically active centers. Even from these new kinetic results it is unfortunately still not possible to precisely determine detailed NH_3 oxidation mechanism (i.e., whether it follows a N_2H_4 route or a two-step SCR-like route). The identification of a dimeric Cu-ion center at lower temperatures clearly makes a NH_2(ads) coupling route possible since each NH_2(ads) can occupy one Cu atom of a dimeric center prior to reaction. On the other hand, extra lattice oxygen (ELO) in these dimeric centers is expected to catalyze NH_3 oxidation to NO more readily. At 350 °C and above, however, NH_2(ads) coupling appears to be unlikely since monomeric Cu ions are the catalytic centers.

Figure 20 presents a direct comparison between Cu- and Fe-SSZ-13 in NH_3 oxidation using samples with Cu/Al = Fe/Al = 0.2 synthesized from the same batch of SSZ-13 substrate (Si/Al = 12).[141] For the Cu-SSZ-13 sample, the largely invariant NH_3 conversions between 300 and 400 °C reinforce the notion on transformation of Cu ion centers in this temperature range discussed above. The Fe-SSZ-13 sample, despite the fact that it contains ~ 40 % dimeric Fe sites even when fully hydrated and is apparently highly active in NO oxidation (Fig. 2) [65], is completely inert in catalyzing NH_3 oxidation below ~ 300 °C. This can be understood from "NH_3 inhibition" of Fe sites that is generally found for Fe-zeolite-based SCR catalysts.[167-171]

4.3. Standard NH_3–SCR

4.3.1. Mechanistic considerations

Reaction mechanisms for standard NH_3-SCR have been extensively studied, yet no general consensus has been reached.[2-8] As described above, the key points of disagreement in the NH_3-SCR mechanism are the following: (1) whether the catalytically relevant Cu/Fe species are monomeric or dimeric (even, perhaps very small oligomeric clusters). (2) Whether NO_2 plays a significant role in the mechanism. (3) Whether redox cycling of the catalytic centers is involved. (4) Whether both Cu/Fe ion sites and Brønsted acid sites collectively provide the catalytic functionality. Depending on whether NO is activated, the reaction can be described to follow an Eley–Rideal (E–R) or a Langmuir–Hinshelwood (L–H) mechanism where in the former, weakly-bound NO reacts with chemisorbed NH_3 to form intermediates that decompose to N_2 while in the latter, NO is required to transform into strongly bound species (e.g., NO_2, nitrite or nitrate moieties) prior to reaction with ammonia. However, a reaction ratio of NH_3/NO = 1/1 and an oxidation state mismatch of N atoms in the reactants (i.e., –3 in NH_3 and +2 in NO) require that the E–R reaction must be accompanied with the reduction of the active centers.

Continuous turnover requires that the reduced active centers be oxidized by O_2. In other words, an E–R mechanism must be coupled with redox steps of the catalytic centers. For the L–H mechanism, redox steps of the catalytic centers are also required; however in this case, catalytic center reduction is accompanied with NO activation. Most of the mechanistic proposals from the literature are reasonable in certain respects. Because of the intrinsic complexity of standard NH_3–SCR described above, it is not unlikely that multiple reaction pathways coexist and their relative significance vary as a function of reaction conditions and catalyst used. However, simultaneous multiple bond cleavage/formation from reactive species on different sites must be considered unlikely in proposing a possible mechanism.

Figure 21 presents a rather general standard SCR mechanism for metal-exchanged zeolite catalysts proposed by Iwasaki, based on a similar one proposed for V_2O_5–based catalysts.[172] This is a typical L–H mechanism coupled with redox of catalytic centers which assumes that (1) reactive ammonia is in the form of NH_4^+; (2) reactive NO_x is in the form of NO_2(ads), formed by NO oxidation by ELO and (3) a dual-site intermediate decomposes to generate N_2. Such a proposal immediately raises debates, e.g., (1) why molecular NH_3 is not chosen as the reactive form of ammonia? (2) why NO has to be oxidized to NO_2(ads)? And (3) why a dual-site instead of a mono-site intermediate that leads to the formation of N_2? In the following these arguments will be addressed to show that such a mechanism is hardly applicable for Cu-CHA catalysts. More plausible ones will be given based on most recent studies.

For Cu-CHA catalysts, Korhonen et al. used operando UV-Vis spectroscopy to first state (without supportive reaction kinetics) that isolated Cu^{2+} ions are the active sites for NH_3-SCR.[173] Recently, Bates et al. discovered a linear correlation between standard SCR rates and *ex situ* UV–Vis–NIR intensities of hydrated Cu(II) d–d transition of their hydrated samples (Si/Al =

4.5); the results are shown in Figure 22.[78] It has also been reported repeatedly that at low to intermediate Cu loadings, isolated Cu^{2+} ions in dehydrated samples are located in the faces of the 6R.[7, 8, 51, 53, 60, 79, 102, 156, 174] It has become rather clear now, therefore, that those isolated Cu^{2+} ions, which stay as Cu^{2+} aqua complexes in fully hydrated samples and "naked" ions near faces of 6R in fully dehydrated samples, are active under SCR reaction conditions. Their nature and location during reaction, however, are not clear due to the limited knowledge thus far learned from *in situ/in operando* spectroscopic studies. Again, as discussed above, no spectroscopic method is expected to be more sensitive than the reactants towards dynamics of the active centers under reaction conditions; at the current stage, kinetics on well-defined catalysts under artifact-free conditions is perhaps the best way to elucidate the nature of active sites under reaction conditions. Nevertheless, *in situ/in operando* spectroscopic studies do reveal two significant findings for elucidating reaction mechanisms. First, *in operando* X-ray absorption studies by Ribeiro and coworkers reveal the coexistence of Cu^{2+} and Cu^{+} under standard SCR conditions.[52, 80, 174] This demonstrates that the redox of active centers is indeed part of the reaction mechanisms. Second, by conducting NO/O_2 titration of adsorbed NH_3 monitored with FTIR, numerous groups realize that molecular NH_3 adsorbed on Cu ion sites is substantially more reactive than NH_4^+.[88, 175, 176] From this standpoint, NH_4^+ should contribute little to SCR.

Whether isolated Cu ions are active centers or not can be probed by kinetic measurements using catalysts with various Cu loadings. In the absence of artifacts (i.e., mass and heat transfer limitations), a linear correlation between reaction rate and Cu content (or invariant turnover frequencies) may be viewed as a proof for isolated Cu ions being the active sites for standard SCR. Gao et al. performed such measurements using Cu-SSZ-13 samples with a wide range of Cu/Al ratios. Figure 23 presents normalized reaction rates (corrected assuming first-order

reaction) as a function of temperature.[152] This graph reveals three distinct kinetic regimes for samples with Cu/Al ≤ 0.11: two normal regimes (≤ 250 °C and ≥ 350 °C) where reaction rates increase with increasing temperature, and an abnormal regime in between where reaction rates *decrease* with increasing temperature. In the high-temperature regime, the invariant TOFs as a function of Cu loading at differential NO conversions displayed in Figure 24 unambiguously confirm that isolated Cu ions are indeed the active centers. At such high temperatures, these active centers are not expected to be solvated and their most probable locations are the faces of 6R. Note that reaction in this regime is characterized with a rather high reaction activation energy of ~140 kJ/mol. In the low-temperature regime, Arrhenius plots are displayed in Figure 25(a) using the following equation (assuming first-order kinetics):

$$k = \frac{r}{[NO]_0} = Ae^{-\frac{E_a}{RT}} \quad (16)$$

In this case, a high degree of complexity as a function of Cu loading is revealed where pre-exponential factors increase orders of magnitude and apparent activation energies increase from ~40 to ~80 kJ/mol as Cu loading rises. Clearly these kinetic variations cannot be justified by assuming a single type of active center at a defined location. Rather, it can be envisioned that Cu ions are sufficiently solvated and mobile at such low temperatures so that transient transformations (e.g., reversible hydrolysis or dimerization of monomers) of Cu-ions are possible and Cu-ions in various forms may contribute to SCR. From the normalized rates and TOFs at a reaction temperature of 185 °C as a function of Cu loading shown in Figure 25(b), the Koros-Nowak criterion can reasonably be considered as obeyed at intermediate Cu loadings (0.044 ≤ Cu/Al ≤ 0.29). In this case, it is reasonable to suggest that SCR is carried out on monomeric Cu-ion active centers, a conclusion also reached by Bates et al.[78] Yet, again, the solvation effects and a basic environment created by stored H_2O/NH_3 make the precise nature of these active centers

undetermined. At very low Cu loadings (Cu/Al < 0.044), a linear correlation between SCR rates and square of Cu loadings suggests, similar to NH_3 oxidation at relatively low temperatures (Figure 19(a)), that the reaction is carried out on dimeric Cu-ion centers.[152] This can be rationalized such that at exceedingly low Cu loadings, either NO activation or Cu-ion monomer redox barriers are formidable so that SCR cannot be catalyzed by a Cu-ion monomer. Reaction kinetics indicate that either by forming transient Cu-ion dimers, or by increasing Cu loading to lower redox barriers could SCR proceeds. Without detailed knowledge on rate-limiting step(s), such explanations can only be judged as tentative. It is clear, however, from the abnormal kinetic regime shown in Figure 23 that the low-temperature active sites "deactivate" with increasing temperature from ~250 to ~350 °C. This is explained such that as the temperature rises, these sites lose extra-framework ligands and migrate to their most stable locations (i.e., faces of 6R) in their dehydrated form, a process that causes their redox barriers to rise. In essence, this abnormal kinetic behavior provides strong evidence to suggest that the low- and high-temperature active monomeric sites are different in their chemical environments. Since it is rather certain that the high-temperature active Cu-ion monomers are located at faces of 6R, a logical conclusion therefore is that the low-temperature active monomers are not located in the same position in contrast to many suggestions.

The assignment Cu-ion monomers as standard SCR active sites casts doubt on a dual-site intermediate mechanism shown in Figure 21 since an expected dual-site intermediate in this case is constructed by an NH_3 adsorbed on a Brønsted acid site (as NH_4^+) and a NO_x species adsorbed on a Cu site. However, this is against the most recent findings that NH_3 adsorbed on Cu ion sites is substantially more reactive than NH_4^+.[88, 175, 176] For a single-site intermediate, the most likely Cu-containing complexes that decompose directly (and stoichiometrically) to N_2 and H_2O should

have one N atom from NH_3 and one N atom from NO_x. Meanwhile, the H:O ratio in such a complex should be 2:1. From these considerations, a nitrosoamide-like complex ($NO–Cu–NH_2$) or an ammonium nitrite-like complex ($NO_2–Cu–NH_4$ or $HNO_2–Cu–NH_3$) appear to be the most probable.[8, 9] Formation of the former can be considered to follow either an E–R or an L–H mechanism while the latter has to be L–H since NO is oxidized. Very recently, Paolucci et al. proposed a standard SCR mechanism in which a nitrosoamide-like complex is involved in the reducing half-cycle and an ammonium nitrite-like complex is involved in the oxidizing half-cycle of a turnover (Figure 26).[80] This study assumes a naked Cu^{2+} monomer located in faces of 6R with two Al T sites as the active center. As discussed above, this is most likely the case for the high-temperature kinetic regime but not necessarily true at low reaction temperatures. Also this model utilizes NH_4^+ as a key reactant species in the oxidizing half-cycle. Other studies suggest that NH_4^+ may not be a very reactive species.[88, 175, 176]

Still, a central point of disagreement among various mechanistic models is how NO is activated, and whether NO_2 formation is indeed important and even a rate-limiting step for standard SCR. NO_2 formation has long been suggested to be a key step in standard SCR and the apparent discrepancy between NO oxidation and standard SCR rates catalyzed by Cu-zeolites (i.e., SCR proceeds much faster than NO oxidation) has long been suggested to be due to a self-poisoning effect by $NO_{2,ads}$ that only applies to NO oxidation.[5] As discussed in the NO oxidation section above, NO_2 inhibition to NO oxidation indeed occurs and appears to be more severe on Cu-zeolites than Fe-zeolites.[157] Yet, a clear mechanism for NO oxidation to $NO_{2,ads}$ catalyzed by isolated Cu ions is not known. Theoretical calculations find that naked Cu^+ and Cu^{2+} ions in faces of 6R bind weakly or not at all to O_2, an essential step in NO oxidation to NO_2.[80, 174] Because of the need to activate O_2, it is conceivable that only Cu/Fe ion dimers or clusters

catalyze NO oxidation to NO_2.[95, 152, 177] Overall, one of the following two scenarios may be considered to understand NO activation in standard SCR catalyzed by Cu-zeolites. First, NO oxidation to $NO_{2,ads}$ may be needed but this is not the rate-limiting step. Second, this chemistry is not even correlated with standard SCR; NO is activated to forms other than $NO_{2,ads}$. These new thoughts have appeared in recent publications and are receiving more support.[8, 153-155] For example, H_2O is known to greatly inhibit gaseous NO_2 formation during NO oxidation. As such, it should also inhibit formation of $NO_{2,ads}$. However, while H_2O mildly inhibits standard SCR over Fe-zeolites,[65] it has no inhibition effect at all to Cu-zeolites.[154]

The discussions above necessitate the following questions: (1) what is the real rate-limiting step for standard SCR catalyzed by isolated Cu ions? (2) How is NO activated prior to the formation of intermediates that decompose to N_2? The answer to the first question is not known, but a few candidates are likely, these include Cu^{2+}/Cu^{+} redox, N–H bond cleavage to generate NH_2(ads), nitrosoamide/ammonium nitrite complex formation, or the formation of a nitrite species that leads to formation of such complexes. From the kinetic data shown in Figures 23 – 25, the existence of multiple kinetic regimes and the variation of activation energies with temperature and Cu loading all indicate that this question may not have an easy answer. Clearly more work is needed, especially theoretical work that is more relevant to realistic reaction conditions.

For the formation of NH_4NO_2 without involving questionable NH_4^+ and $NO_{2,ads}$ as discussed above, the most likely route is an acid-base reaction between NH_3 and HNO_2:

$$NH_3 + HNO_2 = NH_4NO_2 = N_2 + 2H_2O \quad (17)$$

In other words, NO oxidation to HNO_2 without a $NO_{2,ads}$ intermediate is perhaps a key to SCR catalyzed by isolated Cu ions. Moreover, the N atom in HNO_2 has the right oxidation state

(+3) so that charge-transfer between the nitrite complex and the Cu active center becomes unnecessary during its decomposition to form N_2. This should necessarily lower the energy barrier of the overall reaction. Two possible reaction pathways, both involving direct charge-transfer between Cu^{2+} and NO, can realize this chemistry:

$$Cu^{2+} + NO = Cu^{+} - NO^{+} \quad (18)$$

$$NO^{+} + H_2O = H^{+} + HNO_2 \quad (19)$$

$$[Cu(OH)]^{+} + NO = Cu^{+} + HNO_2 \quad (20)$$

Recently Szanyi et al. reported on the formation of NO^+ species during NO chemisorption on Cu-SSZ-13 using FTIR.[178] By applying ^{15}N solid-state MAS-NMR, formation of a Cu^+–NO^+ complex was further confirmed.[155] It is possible that upon its formation, NO^+ can migrate to extra-framework cationic sites to balance negative framework charges.[179] In any case, it is readily conceivable this species can interact with H_2O to generate HNO_2 (eq. 19); this chemistry can then be followed by ammonia nitrite formation and decomposition to N_2. (eq. 17). Based on this, Kwak et al. proposed a rather simple standard SCR mechanism shown in Figure 27.[155] However, NO^+ is only detected in the absence of NH_3.[175] This leaves two possibilities under SCR conditions: (1) NO^+ is consumed immediately upon formation; therefore, it is below the detection limit for FTIR; (2) it is not involved in the presence of NH_3. Again, due to this intrinsic limitation of the FTIR technique, it is not yet possible to fully confirm the proposal shown in Figure 27. Likewise, interaction between NO and a $[Cu(OH)]^+$ site may also generate HNO_2 (eq. 20). This chemistry equally allows one to propose a simple standard SCR mechanism catalyzed by $[Cu(OH)]^+$ that needs further confirmation, for example from theoretical calculations.[152]

So far in this section, focus has been given on low Cu-loaded Cu-CHA catalysts. Although, mobility and interconversion of active sites under reaction conditions bring up certain

complexities, for the most part such catalysts can still be treated as simple catalysts with homogeneous distribution of active sites. For Fe-CHA, or more generally many types of Fe-zeolites, the situation can be much more complicated. For Fe-CHA we are still at the earliest stage of learning. A direct comparison in performance on Cu- and Fe-CHA appears to be a good starting point. Figure 28 displays such a study on samples with Si/Al = 12 and Cu/Al = Fe/Al = 0.2. Both NO and NH_3 conversions are plotted so that SCR selectivities can be readily compared. For the Cu-SSZ-13 catalyst, the light-off temperature is slightly below 200 °C and over the entire temperature ranges investigated here, SCR selectivities are excellent (i.e., NO and NH_3 conversions are essentially equal at all temperatures). In contrast, Fe-SSZ-13 displays no activity below 200 °C and only becomes highly active above ~ 300 °C. To emphasize the key difference, the temperature at 50 % NO conversion (T_{50}) for Cu-SSZ-13 is ~ 120 °C lower than that for Fe-SSZ-13. The poor SCR activity for Fe-CHA at low temperatures can be explained from NH_3 inhibition,[180, 181] an explanation also suitable for the NH_3 oxidation reaction (Figure 20). It is also clear from Figure 28 that, at 275 °C and above, SCR selectivities on Fe-SSZ-13 is ~ 90 % in terms of NH_3 conversion; that is, ~ 10 % NH_3 overconsumption is evident. This will be addressed in the next sub-section.

4.3.2. Non-stoichiometry in standard NH_3-SCR

Under steady-state reaction conditions, NO/NH_3 conversion ratio is expected to be maintained strictly at unity over a selective catalyst. However, this is not always the case; NH_3 (in certain cases NO) overconsumption is frequently found and the causes can range from trivial to rather complicated. One straightforward cause for NH_3 overconsumption is the so-called "non-selective NH_3 oxidation" that has been described above. This typically occurs at relatively high temperatures (~400 °C and above) for samples that are very active in NH_3 oxidation (e.g., high-

Cu loaded samples and samples after hydrothermal aging). Figure 29(a) presents a typical light-off curve on a Cu-SAPO-34 catalyst formed via a solid-state ion exchange method using H-SAPO-34 and CuO.[71] Because of incomplete ion exchange, this catalyst contains both desired isolated Cu^{2+} ions for SCR and undesired CuO particles that catalyze NH_3 oxidation. From this Figure, the NO conversion drop above ~350 °C is due to a decrease in SCR selectivity, caused by NH_3 consumption via oxidation by O_2. For catalysts with low to intermediate Cu loadings, for example a Cu-SSZ-13 catalyst with Si/Al = 6 and Cu/Al = 0.11, light-off curves shown in Figure 29(b) reveal an opposite situation where slight NO overconsumption is realized at temperature intervals between 200–300 and above ~400 °C. Note that this behavior only occurs under SCR conditions (i.e., this catalyst is incapable of catalyzing NO decomposition without the presence of NH_3); and this is due to the participation of NO during Cu^+ oxidation. For example for isolated Cu^+ ions, the following reaction can account for NO overconsumption:[152, 182]

$$4Cu^+ + NO + \frac{1}{2}O_2 + 4H^+ = 4Cu^{2+} + \frac{1}{2}N_2 + 2H_2O \qquad (21)$$

For (transient) Cu-dimers, the reaction may even occur as follows:

$$[Cu^I \cdots Cu^I]^{2+} + 2NO = [Cu^{II}(\mu - O_2)Cu^{II}]^{2+} + N_2 \qquad (22)$$

Although these two reactions account for NO overconsumption, these are clearly not elementary. More details on their mechanisms are not known; however, NO overconsumption greatly supports redox of Cu ions being an essential component of standard SCR.

For Fe-CHA, reaction results shown in Figure 28 reveal another type of NH_3 overconsumption, that is, it occurs at temperatures (e.g., 250–300 °C) at which direct NH_3 oxidation by O_2 does not appear to be likely (Figure 20). This phenomenon is quite common among Fe-zeolites.[183-186] Using isotope labelled reactants, Nedyalkova et al. proposed the existence of an unusual NH_3 oxidation pathway to NO under SCR conditions that account for

NH_3 overconsumption.[187] Since Fe-zeolites are typically much more active in NO oxidation to NO_2, this chemistry could also be rationalized by invoking a NO_2-SCR pathway which will be addressed further below.

4.3.3. Roles of Brønsted acidity in standard NH_3-SCR

Brønsted acidity has an indispensable role in the formation of an active Cu/Fe-ion exchanged zeolite catalyst, that is, it allows atomic dispersion of Cu/Fe ions. Whether or not it plays significant roles in the SCR reaction steps, is, however, heavily debated. All reaction mechanisms that involve an NH_4^+ intermediate favor the argument that Brønsted acidity is important. For V_2O_5-based SCR catalysts, reactive NH_3 in the form of NH_4^+ has been frequently proposed.[10, 188, 189] In explaining the beneficial effects of low Si/Al ratio to SCR on zeolite-based SCR catalysts, Yang and coworkers adapted the same argument and proposed that this is because more NH_4^+ species generate at lower Si/Al ratios (i.e., more Brønsted acid sites).[28, 190] However, as discussed above, recent titration experiments by studies on Cu-CHA catalysts demonstrate that NH_4^+ species are far less reactive toward NO_x than molecular NH_3 adsorbed on Cu sites.[88, 175, 176] Even if the importance of NH_4^+ species is ruled out, as long as redox of active centers is part of the SCR mechanism, H^+ is still indispensable during the Cu^+/Fe^{2+} oxidation step to Cu^{2+}/Fe^{3+} by O_2 when the active centers are monomers. Only for oligomeric active centers can redox occur without the participation of H^+. These two processes are shown below:

$$4M^{n+} + O_2 + 4H^+ = 4M^{(n+1)+} + 2H_2O \quad (23)$$

$$2[M^{n+} \cdots M^{n+}] + O_2 = 2\left[M^{(n+1)+} - O - M^{(n+1)+}\right] \quad (24)$$

In regard to the contribution of Brønsted acidity to SCR rates, it is useful to first consider the following power law model, where α, β, and γ represent the reaction orders for NO, NH_3, and O_2, respectively:

$$-R = Aexp(\frac{-E_a}{RT})[NO]^{\alpha}[NH_3]^{\beta}[O_2]^{\gamma} \quad (25)$$

Studies by numerous groups agree in general that at relatively low temperatures (e.g., < 300 °C), $\alpha \approx 1$, $\beta \approx 0$ and $\gamma \approx 0.5$ over Cu-CHA catalysts.[53, 78] Since under typical SCR reaction conditions, O_2 concentration is in much surplus in comparison to both NO and NH_3, the power-law equation can be simplified as:

$$-R = Aexp(\frac{-E_a}{RT})[NO] \quad (26)$$

From Eq. 26, were there any effects for Brønsted acidity to SCR rates, one expects that either the pre-exponential factor A, or apparent activation energy E_a, or both, varies with H^+ concentration. For Cu-SAPO-34 catalysts, Brønsted acid site density can be systemically varied during the SAPO-34 synthesis step, for example by varying Si content or SDAs.[59, 61, 191, 192] At relatively low Cu loadings, catalysts can be prepared with sufficient differences in Brønsted acid site density. By using such catalysts, Yu et al. discovered that SCR rates increase with increasing H^+ density, yet reaction apparent activation energies do not appear to vary.[176] For Cu-SSZ-13 catalysts, H^+ density can similarly be varied by varying Si/Al ratios of the catalysts. Gao et al. studied low-temperature SCR on low Cu-loaded Cu-SSZ-13 catalysts and results shown in Figure 30 support the beneficial role of H^+ density to SCR rates.[193]

Overall, from the most recent kinetic results on Cu-CHA shown above, and from previous studies on other zeolite catalysts, it appears that a rather general conclusion can be made regarding the role of acidity as pointed out by a few groups, that acidity favors the reaction without being an essential ingredient of the active site and hence the reaction mechanism.[194, 195] Simply put, higher acidity increases NH_3 concentration near active sites. From the power-law equations 25 and 26 shown above, the beneficial role from acidity can be rationalized as caused by increase in exponential factors. From a very recent study by Giordanino et al., $NH_4^+ \cdot nNH_3$

complexes form during NH_3 adsorption on Cu-SSZ-13 and maintain up to ~ 300 °C.[119] Therefore, despite the low reactivity of NH_4^+, it still benefits SCR by attracting more weakly bound NH_3 species.

4.4. Fast and NO_2-SCR: the roles of NO_2

It is of vital importance to recognize two key points for SCR processes involving NO_2 from the gas phase. First, as the average oxidation state for N in NO_x reaches +3 (i.e., NO_2/NO_x = ½), NO activation via redox of the Cu/Fe centers is no longer needed. Indeed, operando XAS measurements under fast and NO_2-SCR conditions reveal, in contrast to standard SCR, that Cu ions permanently stay as Cu^{2+}.[174] Second, as the reaction temperatures become sufficiently high (e.g., above ~ 350 °C), these reactions proceed rapidly enough within the zeolite framework so that even the presence of Cu/Fe centers becomes unnecessary.[5, 196] Figure 31 presents a direct comparison among Cu-, H- and Na-SSZ-13 in fast SCR. Clearly, the presence of Cu^{2+} is vital to NO_x conversions below ~300 °C. At higher temperatures, contribution from Cu^{2+} becomes less significant yet the presence of acidity is still key to high NO_x conversions. These results are, in general, consistent with results obtained from other zeolite catalysts.[5] Therefore, we can state that fast and NO_2-SCR reactions are less sensitive to the type of zeolites and to the nature of cationic sites; as long as the residence time of reactants is sufficiently long, high conversions can be achieved.

Mechanistically, the absence of Cu/Fe ion redox for NO activation, as well as the need to generate NO_x intermediates with a proper N oxidation state of +3 makes the following reactions highly likely:

$$NO + NO_2 = N_2O_3 \quad (27)$$

$$N_2O_3 + H_2O = 2HNO_2 \quad (28)$$

The formation of HNO_2 is thereafter readily followed by the formation of NH_4NO_2 that decomposes to N_2 and H_2O. Such a fast SCR mechanism has been suggested some time ago based on studies with Fe-ZSM-5.[183, 197] It appears that it can be readily adapted for the CHA-based catalysts. It is still not clear whether reaction 27 is carried out in the gas phase, or it is facilitated by the presence of Cu/Fe ions. This uncertainty comes from the possibility that Cu/Fe ions can otherwise promote fast SCR by providing chemisorbed NH_3. The promotion role for acidity can certainly be attributed to the enhancement of residence time for NH_3.

The main side reaction for fast SCR is NO_2-SCR, sometimes referred to as "slow" SCR [8]. The key component that makes this reaction "slow" is NH_4NO_3, an intermediate that is much more stable than NH_4NO_2. According to studies by Tronconi and coworkers,[198, 199] NH_4NO_3 forms from interaction between NH_3 and HNO_3, the latter is generated via NO_2 disproportionation:

$$6NO_2 + 3H_2O = 3HNO_2 + 3HNO_3 \quad (29)$$

$$HNO_3 + NH_3 = NH_4NO_3 \quad (30)$$

NH_4NO_3 can participate in continuous SCR steps to generate N_2 via the following global pathways:[198-200]

$$3NH_4NO_3 + 2NH_3 = 4N_2 + 9H_2O \quad (31)$$

$$NH_4NO_3 + 2NO + 2NH_3 = 2N_2 + 5H_2O \quad (32)$$

The precise elementary reaction steps for these reactions are not clear. It is obvious, however, that these reactions must occur at temperatures where NH_4NO_3 becomes thermally unstable. In this sense, it is expected that CHA-based catalysts are not particularly efficient fast- and NO_2-SCR catalysts since the small pore openings are more readily blocked by NH_4NO_3 deposition. Another key feature for NO_2-SCR is N_2O generation via NH_4NO_3 decomposition:

$$NH_4NO_3 = N_2O + 2H_2O \quad (33)$$

This side reaction has been extensively addressed elsewhere[5] and will not be further discussed.

5. Catalyst stability

One of the primary reasons that Cu-SSZ-13 and Cu-SAPO-34 are chosen commercially as SCR catalysts is their hydrothermal stabilities. There exist a few commonly known reasons to partially interpret their unique stabilities. For example, a Si/Al of ~15 for the current generation of Cu-SSZ-13 can be understood from the fact that higher Si/Al ratio zeolites typically have better stabilities; Cu-SAPO-34 has been chosen since silicoaluminophosphate molecular sieves are typically more refractory than zeolites, etc. However, the most important factor appears to be their small pore openings.[36] Table 1 presents SCR performance (NO_x conversion and N_2O yield, both at 250 °C) for a wide range of fresh and hydrothermally aged (700 °C/24 h or 900 °C/1 h in a flow of 4.5 % H_2O/air mixture) catalysts investigated by researchers at Johnson-Matthey.[36, 42] It is clearly seen that all catalysts with largest pores as 8-membered rings display better hydrothermal stabilities than materials with 10- or 12-membered rings. The fundamentals behind this dramatic difference are not entirely known. One certainly cannot argue that pore opening is the only parameter that plays a role here; for example, the hydrothermally more stable beta has larger pore openings than ZSM-5.

For Cu-SSZ-13, some of the earliest studies suggested that these materials do not even dealuminate.[50, 201] This is somewhat misleading. These materials do dealuminate, albeit under more severe aging conditions as compared to other Cu-zeolites. Lobo and coworkers speculated that during hydrothermal aging, the detached $Al(OH)_3$, owning to its relatively large kinetic diameter, cannot exit the pores of the framework and Al may even reattach back to the

framework.[48] The extent of dealumination is readily probed with solid-state ^{27}Al NMR. Figure 32 presents spectra for a fresh and a hydrothermally aged (HTA) Cu-SSZ-13 sample (Si/Al = 12, Cu/Al = 0.2) where dealumination is manifested by the decrease in tetrahedral Al signal at ~60 ppm. However, the detached Al cannot be detected, a phenomenon common for Cu-zeolites, probably due to the presence of paramagnetic Cu species.[201, 202] Recently, Vennestrøm et al. applied EXAFS to study the nature of the species formed during Cu-zeolite aging. They suggested irreversible formation of catalytically inactive and stable Cu–Al clusters, which have some resemblance to $CuAl_2O_4$.[202] For Cu-SAPO-34 catalysts, formation of similar moieties during aging is also expected.[71]

Since dealumination is initiated from –Si–O(H) –Al– hydrolysis, one might expect that high Cu/Al ratio materials (i.e., materials with minimal residual Brønsted acidity) have the highest hydrothermal stabilities. This is not the case; numerous studies on Cu-CHA formed using various methods (solution ion exchange, one-pot synthesis and solid-state ion exchange) reveal that samples with intermediate Cu/Al ratios display the highest hydrothermal stabilities.[66, 69, 71, 203] It is now generally agreed that at high Cu loadings, the CuO_x clusters generated during high-temperature aging aggressively destroy zeolite structure.[131] In this sense, using certain co-cations to decrease Brønsted acidity of intermediate Cu/Al ratio catalysts may be considered to further improve hydrothermal stabilities.

For use under practical conditions, hydrocarbons and S (fuel-derived contaminants), P and Zn (derived from lubricating oil additives), Ca and Mg (originating from detergent additives), and Pt (derived from the Diesel Oxidation Catalyst) also poison Cu-CHA catalysts.[77] In general, regeneration from such contaminations appears to be relatively simple. The details in these aspects are not included in this review. Excellent summaries can be found elsewhere.[36] For

the much less studied Fe-CHA, more details on their hydrothermal stabilities are not given at this time.

6. Challenges in Automotive Exhaust Control Catalysis

Besides the fundamental and practical issues with respect to the current CHA catalyst discussed in this review, there are a few other general areas which are impacting the practical implementation of the NH_3-SCR technology for vehicle emission control that we briefly discuss here. These relate to the overall emission control system currently being commercialized, as well as continued suitability of the NH_3-SCR technology with respect to some new internal combustion engine (ICE) operational strategies currently under development to meet future vehicle fuel efficiency regulations. In particular, in this closing section we discuss issues with overall emission control system size and weight, NH_3 delivery, and limitations on the low-temperature performance of the current CHA-based NH_3-SCR catalysts. Many of these issues are discussed in more detail elsewhere[204] so are only briefly described here.

6.1. Combined SCR/DPF systems

A recently (model year 2011) commercialized emission control system for the Ford Super Duty diesel pickup truck is shown in Figure 33. As can be seen, this is a large and complicated system that includes a precious-metal based diesel oxidation catalyst (DOC), a urea injection system (diesel emission fluid (DEF) injector), the CHA-zeolite based NH_3-SCR catalyst (note that this is contained on two cordierite monolith substrates), and a diesel particulate filter (DPF). Besides a number of gas sensors, other commercialized systems often also contain an ammonia slip catalyst (ASC) to prevent the emissions of unreacted NH_3. The size and weight of these complex systems causes difficulties for the vehicle manufacturers with weight reducing fuel efficiency and the large system size taking up limited ‘real estate’ needed for many other

components on today's modern vehicles.

One desirable solution to the size and weight issues is to combine some of the functions carried out by the various emission system components, and a combined SCR/DPF has been of particular interest. The DPF is composed of a porous material that allows the exhaust to flow through while trapping the small, ash and carbonaceous-based soot particulates. Instead of coating the NH_3-SCR catalyst on a separate substrate, it is incorporated into the porous DPF material for the combined SCR/DPF system.[205]

A number of issues with such a combined system are clearly evident and are the subject of considerable current research. For example, the NH_3-SCR catalyst will affect the filtering properties of the DPF substrate and care must be taken to minimize detrimental back pressure caused by the catalyst coating while still insuring sufficient NOx reduction performance. In part, this also means determining possible negative effects of the captured soot and ash on reactivity. Furthermore, DPFs need to be periodically regenerated via soot oxidation and this can often lead to locally high temperatures as the soot is combusted. As discussed earlier in this review, the hydrothermal stability of metal-exchanged CHA zeolites is particularly helpful in this regard. With respect to maintaining sufficient NH_3-SCR catalyst performance while also minimizing the amount of the catalyst coating on the filter substrate, the use of small particle or mesoporous[206, 207] zeolites potentially offer some advantage. In particular, typical zeolite particle sizes that are close to 1 micron or more limit the number of reactive sites available during normal operation because the diffusion to the interior of these fairly large particles can be rate-limiting at exhaust flow rates. By using small particle or mesoporous zeolites, it may be possible to reduce the amount of the NH_3-SCR catalyst coating while still maintaining high NOx reduction performance.

6.2. NH_3 delivery

As illustrated in Figure 33, current commercial NH_3-SCR systems provide NH_3 via injection of a urea solution.[208] Upon hydrolysis, the urea molecule can produce two molecules of NH_3 for the downstream SCR reaction with NOx on the zeolite catalyst. Despite the commercial success of this approach for NH_3 delivery, there are several issues with urea solutions that motivate the search for alternatives.[209] These include incomplete decomposition of urea that reduces efficiency and can lead to undesirable deposits that can poison the zeolite catalyst material, and the fact that urea solutions may not be suitable for winter weather in particularly cold climates because they will freeze. Because carrying tanks of ammonia itself is not practical for safety concerns, other chemical precursors for NH_3 delivery are being considered. Solutions of cyanuric acid (a possible decomposition product of urea), and ammonium formate have shown some promise but still have issues in cold winter climates. Solid precursors, including ammonium carbamate, can mitigate the issues with freezing of NH_3 precursor solutions, but there remain difficulties in reliably delivering reproducible amounts of NH_3 that, to date, have prevented commercialization.

Reliable and reproducible ammonia delivery is still a challenge even for urea solutions, leading to low NOx reduction performance or over-dosing of NH_3 that results in NH_3 "slip". Indeed, concerns about NH_3 slip frequently means that vehicle emission control systems that use NH_3 SCR will also incorporate a downstream catalyst that can oxidize NH_3 to N_2. Insufficiently NH_3 delivery, especially at low temperatures, may limit the "light-off" temperatures of the SCR catalyst. This latter issue is important for current applications of the NH_3 SCR technology, but also may be an especially significant limitation for future vehicle NOx emission control as discussed next.

6.3. Low temperature performance for future engine emission control

Looking to the future, highly novel operating modes for internal combustion engines (ICEs) are being researched in order to meet the very stringent new demands for fuel efficiency (e.g., U.S. "CAFE" standards for average miles/gallon are scheduled to increase dramatically over the next 10-15 years). These new ICE engine operation modes, while highly fuel-efficient, result in much lower exhaust temperatures than current engines; temperatures so low that it is hard to imagine how the current catalytic emission control technologies will be able to function.[204] For example, while steady-state operation of the NOx reduction technology at 150 °C may be required[204], current "light-off" temperatures for CHA-based zeolite catalysts are closer to 200 °C as illustrated in Figure 34.[210] Thus, both 'evolutionary' (to address, for example, the above issues discussed earlier in this section) and 'revolutionary' technology development challenges can be foreseen for the catalyst R&D community. Indeed, the catalytic vehicle emission control R&D community is now at the earliest stages of a third era. Having achieved remarkable success in developing the "three-way" catalytic converter (era one) and "lean-NOx" reduction catalyst technologies (era two), the community now faces this new daunting challenge of providing new catalyst materials and processes that can effectively eliminate emissions at these quite low (~150 °C) exhaust temperatures.

For NOx emission control at these low temperatures, it will be especially important to further enhance our fundamental understanding of the NH_3 SCR reaction mechanism over metal-exchanged zeolites, especially with respect to the intrinsic origins of the low-temperature limitations of NOx reduction performance. For example, while the oxidation of NO to NO_2 seems unlikely to be a factor for limiting low temperature NOx reduction over Cu-CHA catalysts, the current uncertainties regarding the mechanism as discussed above prevent a clear

identification of the research target for lowering the "light-off" temperature. However, some potentially promising new results have recently been reported.[211] In particular, Figure 35 shows evidence for "light-off" for standard SCR reaction conditions at temperatures as low as 151 °C. Still, it is clear that a major R&D effort will be needed over at least the next 10 years to realize commercially viable catalytic NOx reduction technologies that reliably operate in this low temperature regime.

7. Concluding remarks

In a comparatively short period of time, Cu-CHA has been introduced into practical applications as the most effective catalyst for NH_3 SCR of NO_x in Diesel engine after-treatment due to its excellent lean NO_x reduction activity, superior N_2 selectivity and remarkably high hydrothermal stability. The success of this catalyst came at a time when many believed that zeolite-based catalysts would never meet the stringent performance and stability requirements for practical applications. Some of our current understanding of Cu-CHA materials comes from the considerable literature over the past thirty years on other zeolite-based catalysts, in particular on Cu(Fe)-ZSM-5 and Cu(Fe)-beta. Still, the understanding of the working catalyst has been greatly enhanced by the availability of a number of new *in situ/in operando* spectroscopy techniques that provided simultaneous information on the oxidation state and location of Cu ions, the nature of adsorbed species present in the catalyst and catalytic performance. Despite extensive recent research on the Cu-CHA catalysts, there are a number of unanswered questions remaining; namely, what is the role of NO^+ in the reaction mechanism, do proton sites of the zeolite play a role in the overall catalytic cycle, which Cu ions are the true active site under low and high temperature NO_x reduction conditions, and what provides these catalysts the observed superior hydrothermal stability? Although a number of reaction mechanisms have been

proposed for the NH_3 SCR of NO_x over these catalysts, none of them is able to completely explain the full catalytic cycle over the entire range of operating temperatures. Addressing these issues in the future may lead to the development of NO_x reduction catalysts with even better performance, mainly at the lower end of the required operating temperature (<200 °C).

Author Contributions

The manuscript was written through contributions of all authors. All authors have given approval to the final version of the manuscript.

Funding

A.M.B. and I.L.G. would like to thank EPSRC for funding. F.G., C.H.F.P. and J.Sz. gratefully acknowledge financial support from the US Department of Energy (DOE), Office of Energy Efficiency and Renewable Energy, Vehicle Technologies Program.

Notes

The authors declare no competing financial interest.

Biographies

Dr. Andrew M. Beale studied chemistry at Sussex University and got his PhD in 2003 from the Royal Institution of Great Britain/University College London with Profs. G. Sankar and C. Richard A. Catlow. In 2004 he moved to the department of Inorganic Chemistry and Catalysis, Utrecht University in the Netherlands first as a post-doctoral fellow and subsequently (2009) as Assistant Professor in the group of Prof. Bert M. Weckhuysen. In 2013 he moved to the department of chemistry at UCL as an EPSRC Early Career Fellow and Lecturer. His work focuses on establishing structure-function relationships in catalytic solids as a function of both time and space and is the author of over 100 publications.

Dr. Feng Gao received his undergraduate degree in Chemical Engineering from Tianjin University, China, in 1994. He obtained a Ph.D. in Physical Chemistry in 2004 from the University of Wisconsin-Milwaukee under Prof. Wilfred T. Tysoe. From 2007 to 2009, he was a postdoc at Texas A&M University under Prof. D. Wayne Goodman. He spent 2 years as a research staff at Washington State University before joining Pacific Northwest National Laboratory (PNNL) as a staff scientist in 2011, conducting research in basic and environmental heterogeneous catalysis. He is a coauthor of 80+ publications.

Dr. Inés Lezcano-Gonzalez studied Chemical Engineering at the University of Valencia and received her PhD in chemistry at the Institute of Chemical Technology (ITQ) under the guidance of Dr. Teresa Blasco, in 2011 (Polytechnic University of Valencia). After three years of postdoctoral research at Utrecht University with Prof. Bert M. Weckhuysen, she joined the department of chemistry at University

College London and the UK Catalysis Hub, where she is currently working as a postdoctoral research associate in the group of Dr. Andrew M. Beale. Her research interests lie in the field of heterogeneous catalysis, mainly on the application of in situ and operando spectroscopic techniques.

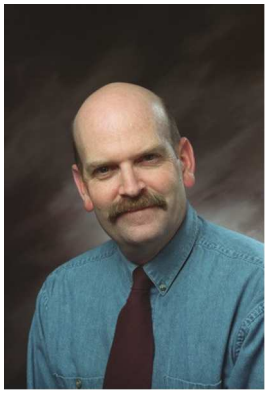

Dr. Charles H.F. Peden completed his undergraduate degree in Chemistry from California State University, Chico, in 1978, and then obtained his Ph.D. in Physical Chemistry from University of California, Santa Barbara in 1983. After a 2-year post-doctoral tenure with D. Wayne Goodman at Sandia National Laboratories, he joined the scientific staff at Sandia. He moved to Pacific Northwest National Laboratory in 1992 and is now a Laboratory Fellow and Associate Director of the Institute for Integrated Catalysis at PNNL. Dr. Peden has over 250 peer-reviewed publications on the catalytic properties of metal and metal-oxide materials, including their use for catalytic vehicle emission control.

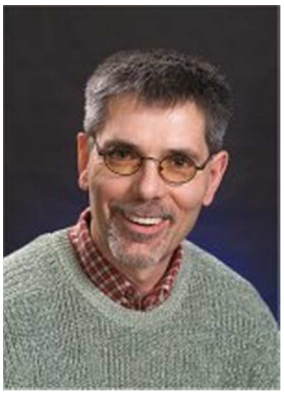

Dr. János Szanyi received his undergraduate (1982) and Dr.Univ. (1986) degrees from the University of Szeged, Hungary, and his Ph.D. degree at Texas A&M University from Prof. D. Wayne Goodman`s group in 1993. After post-graduate work with Prof. Jack H. Lunsford at TAMU, and with Dr. Mark T. Paffett at Los Alamos National Laboratory, he joined the technical staff at PPG Industries in Pittsburgh, PA in 1996. Since 2001 Dr. Szanyi has been conducting research at the Pacific Northwest National Laboratory in the field of environmental catalysis focusing on understanding structure-reactivity relationships and reaction mechanisms over model and practical heterogeneous catalysts. He has co-authored over 130 peer-reviewed publications.

Abbreviations:
SCR: selective catalytic reduction
NSR: NOx storage/reduction
DPF: Diesel particulate filter
DOC: Diesel oxidation catalyst
ASC: ammonia slip catalyst
ICE: internal combustion engine
CHA: chabasite
SDA: structure directing agent
TEPA: tetraethylenepentamine
SSIE: solid-state ion exchange
6R: six-member ring
8R: eight-member ring
D6R: double six-member ring
EFAl: extra framework aluminum
ELO: extra lattice oxygen
XANES: X-ray absorption near edge structure
EXAFS: extended X-ray absorption fine structure
HERFD: high resolution fluorescence detection

V2C: valence-to-core
XRD: X-ray diffraction
IR: infrared
FTIR: Fourier transform infrared
DRIFTS: diffuse reflectance infrared Fourier transform spectroscopy
UV-Vis: ultraviolet-visible
LMCT: ligand-to-metal charge transfer
MAS NMR: magic angle spinning nuclear magnetic resonance
EPR: electron paramagnetic resonance
TPD: temperature programmed desorption
TPR: temperature programmed reduction
DFT: Density functional theory
HTA: hydrothermal ageing
E-R: Eley-Rideal
L-H: Langmuir-Hinshelwood

References

1. R. M. Heck, R. J. Farrauto and S. T. Gulati, *Catalytic Air Pollution Control: Commercial Technology, 3rd Edition*, Wiley, New York, 2009.
2. V. I. Parvulescu, P. Grange and B. Delmon, *Catal Today*, 1998, 46, 233-316.
3. G. Busca, M. A. Larrubia, L. Arrighi and G. Ramis, *Catal Today*, 2005, 107-08, 139-148.
4. Z. M. Liu and S. I. Woo, *Catal Rev*, 2006, 48, 43-89.
5. S. Brandenberger, O. Krocher, A. Tissler and R. Althoff, *Catal Rev*, 2008, 50, 492-531.
6. B. Moden, J. M. Donohue, W. E. Cormier and H. X. Li, *Top Catal*, 2010, 53, 1367-1373.
7. U. Deka, I. Lezcano-Gonzalez, B. M. Weckhuysen and A. M. Beale, *Acs Catal*, 2013, 3, 413-427.
8. F. Gao, J. H. Kwak, J. Szanyi and C. H. F. Peden, *Top Catal*, 2013, 56, 1441-1459.
9. G. Centi and S. Perathoner, *Appl Catal a-Gen*, 1995, 132, 179-259.
10. G. Busca, L. Lietti, G. Ramis and F. Berti, *Appl Catal B-Environ*, 1998, 18, 1-36.
11. H. Bosch and F. J. J. G. Janssen, *Catal Today*, 1988, 2, 369-531.
12. J. W. Byrne, J. M. Chen and B. K. Speronello, *Catal Today*, 1992, 13, 33-42.
13. J. Jansson, in *Urea-SCR Technology for deNOx After Treatment of Diesel Exhausts*, eds. I. Nova and E. Tronconi, Springer Science and Business Media, New York, 2014, ch. 3, pp. 65-96.
14. M. Iwamoto, H. Furukawa, Y. Mine, F. Uemura, S. I. Mikuriya and S. Kagawa, *J Chem Soc Chem Comm*, 1986, DOI: Doi 10.1039/C39860001272, 1272-1273.
15. C. T. Goralski and W. F. Schneider, *Appl Catal B-Environ*, 2002, 37, 263-277.
16. T. Komatsu, M. Nunokawa, I. S. Moon, T. Takahara, S. Namba and T. Yashima, *J Catal*, 1994, 148, 427-437.
17. F. Witzel, G. A. Sill and W. K. Hall, *J Catal*, 1994, 149, 229-237.
18. K. C. C. Kharas, D. J. Liu and H. J. Robota, *Catal Today*, 1995, 26, 129-145.
19. G. D. Lei, B. J. Adelman, J. Sarkany and W. M. H. Sachtler, *Appl Catal B-Environ*, 1995, 5, 245-256.
20. K. C. C. Kharas, H. J. Robota and D. J. Liu, *Appl Catal B-Environ*, 1993, 2, 225-237.
21. J. Y. Yan, G. D. Lei, W. M. H. Sachtler and H. H. Kung, *J Catal*, 1996, 161, 43-54.
22. X. B. Feng and W. K. Hall, *Catal Lett*, 1996, 41, 45-46.
23. X. B. Feng and W. K. Hall, *J Catal*, 1997, 166, 368-376.
24. R. W. Joyner and M. Stockenhuber, *Catal Lett*, 1997, 45, 15-19.
25. T. V. Voskoboinikov, H. Y. Chen and W. M. H. Sachtler, *Appl Catal B-Environ*, 1998, 19, 279-287.

26. P. Marturano, L. Drozdova, A. Kogelbauer and R. Prins, *J Catal*, 2000, 192, 236-247.
27. R. Q. Long and R. T. Yang, *Catal Lett*, 2001, 74, 201-205.
28. R. Q. Long and R. T. Yang, *J Catal*, 1999, 188, 332-339.
29. R. Q. Long and R. T. Yang, *J Am Chem Soc*, 1999, 121, 5595-5596.
30. B. Coq, M. Mauvezin, G. Delahay, J. B. Butet and S. Kieger, *Appl Catal B-Environ*, 2000, 27, 193-198.
31. B. Coq, M. Mauvezin, G. Delahay and S. Kieger, *J Catal*, 2000, 195, 298-303.
32. M. Mauvezin, G. Delahay, B. Coq, S. Kieger, J. C. Jumas and J. Olivier-Fourcade, *J Phys Chem B*, 2001, 105, 928-935.
33. A. M. Frey, S. Mert, J. Due-Hansen, R. Fehrmann and C. H. Christensen, *Catal Lett*, 2009, 130, 1-8.
34. D. Klukowski, P. Balle, B. Geiger, S. Wagloehner, S. Kureti, B. Kimmerle, A. Baiker and J. D. Grunwaldt, *Appl Catal B-Environ*, 2009, 93, 185-193.
35. C. H. F. Peden, J. H. Kwak, S. D. Burton, R. G. Tonkyn, D. H. Kim, J. H. Lee, H. W. Jen, G. Cavataio, Y. S. Cheng and C. K. Lambert, *Catal Today*, 2012, 184, 245-251.
36. H. Y. Chen, in *Urea-SCR Technology for deNOx After Treatment of Diesel Exhausts*, eds. I. Nova and E. Tronconi, Springer Science and Business Media, New York, 2014, ch. 5, pp. 123-147.
37. J. F. Haw, W. G. Song, D. M. Marcus and J. B. Nicholas, *Accounts Chem Res*, 2003, 36, 317-326.
38. J. Q. Chen, A. Bozzano, B. Glover, T. Fuglerud and S. Kvisle, *Catal Today*, 2005, 106, 103-107.
39. S. Bordiga, L. Regli, D. Cocina, C. Lamberti, M. Bjorgen and K. P. Lillerud, *J Phys Chem B*, 2005, 109, 2779-2784.
40. S. Bordiga, L. Regli, C. Lamberti, A. Zecchina, M. Bjorgen and K. P. Lillerud, *J Phys Chem B*, 2005, 109, 7724-7732.
41. Y. Jeanvoine, J. G. Angyan, G. Kresse and J. Hafner, *J Phys Chem B*, 1998, 102, 5573-5580.
42. J. Andersen, J. E. Bailie, J. L. Casci, H. Y. Chen, J. M. Fedeyko, R. K. S. Foo and R. R. Rajaram, *International Patent*, 2008, WO/2008/132452.
43. I. Bull, W. M. Xue, P. Burk, R. S. Boorse, W. M. Jaglowski, G. S. Koermer, A. Moini, J. A. Patchett, J. C. Dettling and M. T. Caudle, *US Patent*, 2009, 7601662B2.
44. I. Bull, A. Mioni, G. S. Koermer, J. A. Patchett, W. M. Jaglowski and S. Roth, *US Patent*, 2010, 7,704,475 B2.
45. P. J. Andersen, H. Y. Chen, J. M. Fedeyko and E. Weigert, *US Patent*, 2011, 7,998,443 B2.
46. L. S. Dent and J. V. Smith, *Nature*, 1958, 181, 1794-1796.
47. S. I. Zones, *US Patent*, 1985, 4,544,538.
48. J. H. Kwak, R. G. Tonkyn, D. H. Kim, J. Szanyi and C. H. F. Peden, *J Catal*, 2010, 275, 187-190.
49. D. W. Fickel and R. F. Lobo, *J Phys Chem C*, 2010, 114, 1633-1640.
50. D. W. Fickel, E. D'Addio, J. A. Lauterbach and R. F. Lobo, *Appl Catal B-Environ*, 2011, 102, 441-448.
51. U. Deka, A. Juhin, E. A. Eilertsen, H. Emerich, M. A. Green, S. T. Korhonen, B. M. Weckhuysen and A. M. Beale, *Journal of Physical Chemistry C*, 2012, 116, 4809-4818.
52. V. F. Kispersky, A. J. Kropf, F. H. Ribeiro and J. T. Miller, *Physical Chemistry Chemical Physics*, 2012, 14, 2229-2238.
53. F. Gao, E. D. Walter, E. M. Karp, J. Y. Luo, R. G. Tonkyn, J. H. Kwak, J. Szanyi and C. H. F. Peden, *J Catal*, 2013, 300, 20-29.
54. M. Briend, R. Vomscheid, M. J. Peltre, P. P. Man and D. Barthomeuf, *J Phys Chem-Us*, 1995, 99, 8270-8276.
55. I. Bull and U. Muller, *European Patent*, 2011, 2269733.
56. T. Alvaro-Munoz, C. Marquez-Alvarez and E. Sastre, *Catal Today*, 2012, 179, 27-34.
57. S. Wilson and P. Barger, *Micropor Mesopor Mat*, 1999, 29, 117-126.

58. R. Vomscheid, M. Briend, M. J. Peltre, P. P. Man and D. Barthomeuf, *J Phys Chem-Us*, 1994, 98, 9614-9618.
59. F. Gao, E. D. Walter, N. M. Washton, J. Szanyi and C. H. F. Peden, *Acs Catal*, 2013, 3, 2083-2093.
60. L. Wang, W. Li, G. S. Qi and D. Weng, *J Catal*, 2012, 289, 21-29.
61. J. Wang, T. Yu, X. Q. Wang, G. S. Qi, J. J. Xue, M. Q. Shen and W. Li, *Appl Catal B-Environ*, 2012, 127, 137-147.
62. A. Frache, B. I. Palella, M. Cadoni, R. Pirone, H. O. Pastore and L. Marchese, *Top Catal*, 2003, 22, 53-57.
63. D. B. Akolekar, S. K. Bhargava and K. Foger, *J Chem Soc Faraday T*, 1998, 94, 155-160.
64. D. B. Akolekar and S. K. Bhargava, *Appl Catal a-Gen*, 2001, 207, 355-365.
65. F. Gao, M. Kollár, R. K. Kukkadapu, N. M. Washton, Y. L. Wang, J. Szanyi and C. H. F. Peden, *Appl Catal B-Environ*, 2015, 164, 407-419.
66. L. M. Ren, L. F. Zhu, C. G. Yang, Y. M. Chen, Q. Sun, H. Y. Zhang, C. J. Li, F. Nawaz, X. J. Meng and F. S. Xiao, *Chem Commun*, 2011, 47, 9789-9791.
67. L. J. Xie, F. D. Liu, L. M. Ren, X. Y. Shi, F. S. Xiao and H. He, *Environ Sci Technol*, 2014, 48, 566-572.
68. R. Martinez-Franco, M. Moliner, C. Franch, A. Kustov and A. Corma, *Appl Catal B-Environ*, 2012, 127, 273-280.
69. R. Martinez-Franco, M. Moliner, P. Concepcion, J. R. Thogersen and A. Corma, *J Catal*, 2014, 314, 73-82.
70. D. Wang, F. Gao, C. H. F. Peden, J. H. Li, K. Kamasamudram and W. S. Epling, *Chemcatchem*, 2014, 6, 1579-1583.
71. F. Gao, E. D. Walter, N. M. Washton, J. Szanyi and C. H. F. Peden, *Appl Catal B-Environ*, 2015, 162, 501-514.
72. S. Shwan, M. Skoglundh, L. F. Lundegaard, R. R. Tiruvalam, T. V. W. Janssens, A. Carlsson and P. N. R. Vennestrøm, *Acs Catal*, 2015, 5, 16-19.
73. S. Bordiga, E. Groppo, G. Agostini, J. A. van Bokhoven and C. Lamberti, *Chem. Rev.*, 2013, 113, 1736-1850.
74. J. G. Mesu, T. Visser, A. M. Beale, F. Soulimani and B. M. Weckhuysen, *Chemistry-a European Journal*, 2006, 12, 7167-7177.
75. J. H. Kwak, T. Varga, C. H. F. Peden, F. Gao, J. C. Hanson and J. Szanyi, *Journal of Catalysis*, 2014, 314, 83-93.
76. E. Borfecchia, K. A. Lomachenko, F. Giordanino, H. Falsig, P. Beato, A. V. Soldatov, S. Bordiga and C. Lamberti, *Chemical Science*, 2015, 6, 548-563.
77. I. Lezcano-Gonzalez, U. Deka, H. E. van der Bij, P. Paalanen, B. Arstad, B. M. Weckhuysen and A. M. Beale, *Appl Catal B-Environ*, 2014, 154, 339-349.
78. S. A. Bates, A. A. Verma, C. Paolucci, A. A. Parekh, T. Anggara, A. Yezerets, W. F. Schneider, J. T. Miller, W. N. Delgass and F. H. Ribeiro, *Journal of Catalysis*, 2014, 312, 87-97.
79. U. Deka, I. Lezcano-Gonzalez, S. J. Warrender, A. L. Picone, P. A. Wright, B. M. Weckhuysen and A. M. Beale, *Microporous and Mesoporous Materials*, 2013, 166, 144-152.
80. C. Paolucci, A. A. Verma, S. A. Bates, V. F. Kispersky, J. T. Miller, R. Gounder, W. N. Delgass, F. H. Ribeiro and W. F. Schneider, *Angew Chem Int Edit*, 2014, 53, 11828-11833.
81. P. Glatzel and U. Bergmann, *Coordination Chemistry Reviews*, 2005, 249, 65-95.
82. S. T. Korhonen, D. W. Fickel, R. F. Lobo, B. M. Weckhuysen and A. M. Beale, *Chemical Communications*, 2011, 47, 800-802.
83. K. Kervinen, P. C. A. Bruijnincx, A. M. Beale, J. G. Mesu, G. van Koten, R. Gebbink and B. M. Weckhuysen, *Journal of the American Chemical Society*, 2006, 128, 3208-3217.
84. J. G. Mesu, T. Visser, F. Soulimani, E. E. van Faassen, P. de Peinder, A. M. Beale and B. M. Weckhuysen, *Inorganic Chemistry*, 2006, 45, 1960-1971.

85. A. M. Beale, E. K. Gibson, M. G. O'Brien, S. D. M. Jacques, R. J. Cernik, M. Di Michiel, P. D. Cobden, O. Pirgon-Galin, L. van de Water, M. J. Watson and B. M. Weckhuysen, *Journal of Catalysis*, 2014, 314, 94-100.
86. D. W. Fickel, J. M. Fedeyko and R. F. Lobo, *Journal of Physical Chemistry C*, 2010, 114, 1633-1640.
87. C. W. Andersen, M. Bremholm, P. N. R. Vennestrom, A. B. Blichfeld, L. F. Lundegaard and B. B. Iversen, *IUCrJ*, 2014, 1, 382-386.
88. I. Lezcano-Gonzalez, U. Deka, B. Arstad, A. Van Yperen-De Deyne, K. Hemelsoet, M. Waroquier, V. Van Speybroeck, B. M. Weckhuysen and A. M. Beale, *Phys Chem Chem Phys*, 2014, 16, 1639-1650.
89. W. A. Slawniski, D. S. Wragg, D. Akporiaye and H. Fjellvag, *Microporous and Mesoporous Materials*, 2014, 195, 311-318.
90. US2010028679-A1; US7914760-B2, 2010.
91. WO2014038636-A1; JP2014065029-A; JP2014080345-A, 2014.
92. J. Wang, Z. Peng, H. Qiao, L. Han, W. Bao, L. Chang, G. Feng and W. Liu, *Rsc Advances*, 2014, 4, 42403-42411.
93. R. A. Schoonheydt, *Chem. Soc. Rev.*, 2010, 39, 5051-5066.
94. F. Giordanino, P. N. R. Vennestrom, L. F. Lundegaard, F. N. Stappen, S. Mossin, P. Beato, S. Bordiga and C. Lamberti, *Dalton T*, 2013, 42, 12741-12761.
95. A. A. Verma, S. A. Bates, T. Anggara, C. Paolucci, A. A. Parekh, K. Kamasamudram, A. Yezerets, J. T. Miller, W. N. Delgass, W. F. Schneider and F. H. Ribeiro, *Journal of Catalysis*, 2014, 312, 179-190.
96. A. Vimont, F. Thibault-Starzyk and M. Daturi, *Chem. Soc. Rev.*, 2010, 39, 4928-4950.
97. C. Lamberti, A. Zecchina, E. Groppo and S. Bordiga, *Chem. Soc. Rev.*, 2010, 39, 4951-5001.
98. K. Hadjiivanov and H. Knözinger, *Surface Science*, 2009, 603, 1629-1636.
99. J. Hun Kwak, H. Zhu, J. H. Lee, C. H. F. Peden and J. Szanyi, *Chemical Communications*, 2012, 48, 4758-4760.
100. J. Szanyi, J. H. Kwak, H. Zhu and C. H. F. Peden, *Physical Chemistry Chemical Physics*, 2013, 15, 2368-2380.
101. F. Giordanino, P. N. R. Vennestrom, L. F. Lundegaard, F. N. Stappen, S. Mossin, P. Beato, S. Bordiga and C. Lamberti, *Dalton Transactions*, 2013, 42, 12741-12761.
102. F. Goltl, R. E. Bulo, J. Hafner and P. Sautet, *J Phys Chem Lett*, 2013, 4, 2244-2249.
103. F. Gao, M. Kollár, R. K. Kukkadapu, N. M. Washton, Y. Wang, J. Szanyi and C. H. F. Peden, *Applied Catalysis B: Environmental*, 2015, 164, 407-419.
104. M. Mihaylov, E. Ivanova, N. Drenchev and K. Hadjiivanov, *The Journal of Physical Chemistry C*, 2009, 114, 1004-1014.
105. H. Knözinger, *Handbook of Heterogeneous Catalysis*, Springer-Verlag, Inc., 1996.
106. J. H. Kwak, J. H. Lee, S. D. Burton, A. S. Lipton, C. H. F. Peden and J. Szanyi, *Angewandte Chemie International Edition*, 2013, 52, 9985-9989.
107. R. Zhang, J.-S. McEwen, M. Kollár, F. Gao, Y. Wang, J. Szanyi and C. H. F. Peden, *ACS Catalysis*, 2014, 4, 4093-4105.
108. R. Kefirov, E. Ivanova, K. Hadjiivanov, S. Dzwigaj and M. Che, *Catal Lett*, 2008, 125, 209-214.
109. L. Benco, T. Bucko, R. Grybos, J. Hafner, Z. Sobalik, J. Dedecek, S. Sklenak and J. Hrusak, *The Journal of Physical Chemistry C*, 2007, 111, 9393-9402.
110. G. Mul, J. Pérez-Ramírez, F. Kapteijn and J. A. Moulijn, *Catal Lett*, 2002, 80, 129-138.
111. M. Rivallan, G. Ricchiardi, S. Bordiga and A. Zecchina, *Journal of Catalysis*, 2009, 264, 104-116.
112. G. Berlier, G. Spoto, G. Ricchiardi, S. Bordiga, C. Lamberti and A. Zecchina, *Journal of Molecular Catalysis A: Chemical*, 2002, 182–183, 359-366.

113. R. Joyner and M. Stockenhuber, *The Journal of Physical Chemistry B*, 1999, 103, 5963-5976.
114. M. P. Ruggeri, I. Nova, E. Tronconi, J. A. Pihl, T. J. Toops and W. P. Partridge, *Applied Catalysis B: Environmental*, 2015, 166–167, 181-192.
115. L. Xie, F. Liu, K. Liu, X. Shi and H. He, *Catalysis Science & Technology*, 2014, 4, 1104-1110.
116. L. Ma, Y. Cheng, G. Cavataio, R. W. McCabe, L. Fu and J. Li, *Applied Catalysis B: Environmental*, 2014, 156–157, 428-437.
117. Y. J. Kim, J. K. Lee, K. M. Min, S. B. Hong, I.-S. Nam and B. K. Cho, *Journal of Catalysis*, 2014, 311, 447-457.
118. H. Zhu, J. H. Kwak, C. H. F. Peden and J. Szanyi, *Catalysis Today*, 2013, 205, 16-23.
119. F. Giordanino, E. Borfecchia, K. A. Lomachenko, A. Lazzarini, G. Agostini, E. Gallo, A. V. Soldatov, P. Beato, S. Bordiga and C. Lamberti, *J Phys Chem Lett*, 2014, 5, 1552-1559.
120. F. Gao, Y. L. Wang and D. W. Goodman, *J Phys Chem C*, 2009, 113, 14993-15000.
121. X. Yang, Z. Wu, M. Moses-Debusk, D. R. Mullins, S. M. Mahurin, R. A. Geiger, M. Kidder and C. K. Narula, *The Journal of Physical Chemistry C*, 2012, 116, 23322-23331.
122. R. Zhang, Y. Li and T. Zhen, *RSC Advances*, 2014, 4, 52130-52139.
123. J. Sárkány and W. M. H. Sachtler, *Zeolites*, 1994, 14, 7-11.
124. J. Sárkány and W. M. H. Sachtler, in *Studies in Surface Science and Catalysis*, eds. H. G. K. I. K. H.K. Beyer and J. B. Nagy, Elsevier, 1995, vol. Volume 94, pp. 649-656.
125. G. D. Lei, B. J. Adelman, J. Sárkány and W. M. H. Sachtler, *Applied Catalysis B: Environmental*, 1995, 5, 245-256.
126. J. Sárkány, *Journal of Molecular Structure*, 1997, 410–411, 95-98.
127. J. Sárkány, *Journal of Molecular Structure*, 1997, 410–411, 137-140.
128. J. Sárkány, *Journal of Molecular Structure*, 1997, 410–411, 145-148.
129. J. Sárkány, *Applied Catalysis A: General*, 1999, 188, 369-379.
130. J. Sárkány, *Applied Catalysis A: General*, 2002, 229, 291-312.
131. J. Sárkány, *Surface Science*, 2004, 566–568, Part 2, 723-727.
132. D. Goldfarb, *Electron Paramagnetic Resonance. A Practitioner's Toolkit*, John Wiley & Sons, Inc., 2009.
133. Y. Li, Z. H. Wei, J. M. Sun, F. Gao, C. H. F. Peden and Y. Wang, *J Phys Chem C*, 2013, 117, 5722-5729.
134. F. Gao, E. D. Walter, M. Kollar, Y. Wang, J. Szanyi and C. H. F. Peden, *Journal of Catalysis*, 2014, 319, 1-14.
135. A. Godiksen, F. N. Stappen, P. N. R. Vennestrøm, F. Giordanino, S. B. Rasmussen, L. F. Lundegaard and S. Mossin, *The Journal of Physical Chemistry C*, 2014, 118, 23126-23138.
136. Q. Guo, F. Fan, D. A. J. M. Ligthart, G. Li, Z. Feng, E. J. M. Hensen and C. Li, *ChemCatChem*, 2014, 6, 634-639.
137. L. Ma, Y. Cheng, G. Cavataio, R. W. McCabe, L. Fu and J. Li, *Chemical Engineering Journal*, 2013, 225, 323-330.
138. L. Mafra, J. A. Vidal-Moya and T. Blasco, *Annual Reports on NMR Spectroscopy*, Elsevier, 2012.
139. J. H. Kwak, D. Tran, S. D. Burton, J. Szanyi, J. H. Lee and C. H. F. Peden, *Journal of Catalysis*, 2012, 287, 203-209.
140. S. J. Schmieg, S. H. Oh, C. H. Kim, D. B. Brown, J. H. Lee, C. H. F. Peden and D. H. Kim, *Catalysis Today*, 2012, 184, 252-261.
141. F. Gao, Y. L. Wang, M. Kollar, N. M. Washton, J. Szanyi and C. H. F. Peden, *Catal Today*, 2015, in press.
142. I. Lezcano-Gonzalez, U. Deka, H. E. van der Bij, P. Paalanen, B. Arstad, B. M. Weckhuysen and A. M. Beale, *Applied Catalysis B: Environmental*, 2014, 154–155, 339-349.

143. U. Deka, I. Lezcano-Gonzalez, S. J. Warrender, A. Lorena Picone, P. A. Wright, B. M. Weckhuysen and A. M. Beale, *Microporous and Mesoporous Materials*, 2013, 166, 144-152.
144. A. Corma, *Chem. Rev.*, 1995, 95, 559-614.
145. F. Lónyi and J. Valyon, *Microporous and Mesoporous Materials*, 2001, 47, 293-301.
146. E.-Y. Choi, I.-S. Nam and Y. G. Kim, *Journal of Catalysis*, 1996, 161, 597-604.
147. M. Niwa, S. Nishikawa and N. Katada, *Microporous and Mesoporous Materials*, 2005, 82, 105-112.
148. D. Wang, L. Zhang, K. Kamasamudram and W. S. Epling, *Acs Catal*, 2013, 3, 871-881.
149. H. Sjovall, R. J. Blint and L. Ollsson, *J Phys Chem C*, 2009, 113, 1393-1405.
150. O. Mihai, C. R. Widyastuti, S. Andonova, K. Kamasamudram, J. H. Li, S. Y. Joshi, N. W. Currier, A. Yezerets and L. Olsson, *J Catal*, 2014, 311, 170-181.
151. D. Wang, Y. Jangjou, Y. Liu, M. K. Sharma, J. Luo, J. Li, K. Kamasamudram and W. S. Epling, *Applied Catalysis B: Environmental*, 2015, 165, 438-445.
152. F. Gao, E. D. Walter, M. Kollar, Y. L. Wang, J. Szanyi and C. H. F. Peden, *J Catal*, 2014, 319, 1-14.
153. I. Ellmers, R. P. Velez, U. Bentrup, A. Bruckner and W. Grunert, *J Catal*, 2014, 311, 199-211.
154. M. Ruggeri, I. Nova and E. Tronconi, *Top Catal*, 2013, 56, 109-113.
155. J. H. Kwak, J. H. Lee, S. D. Burton, A. S. Lipton, C. H. F. Peden and J. Szanyi, *Angew Chem Int Edit*, 2013, 52, 9985-9989.
156. A. Godiksen, F. N. Stappen, P. N. R. Vennestrom, F. Giordanino, S. B. Rasmussen, L. F. Lundegaard and S. Mossin, *J Phys Chem C*, 2014, 118, 23126-23138.
157. P. S. Metkar, V. Balakotaiah and M. P. Harold, *Catal Today*, 2012, 184, 115-128.
158. G. Ramis, L. Yi and G. Busca, *Catal Today*, 1996, 28, 373-380.
159. N. N. Sazonova, A. V. Simakov, T. A. Nikoro, G. B. Barannik, V. F. Lyakhova, V. I. Zheivot, Z. R. Ismagilov and H. Veringa, *React Kinet Catal L*, 1996, 57, 71-79.
160. M. Ueshima, K. Sano, M. Ikeda, K. Yoshino and J. Okamura, *Res Chem Intermediat*, 1998, 24, 133-141.
161. R. Q. Long and R. T. Yang, *J Catal*, 2001, 201, 145-152.
162. G. S. Qi, J. E. Gatt and R. T. Yang, *J Catal*, 2004, 226, 120-128.
163. G. S. Qi and R. T. Yang, *Appl Catal a-Gen*, 2005, 287, 25-33.
164. M. Amblard, R. Burch and B. W. L. Southward, *Catal Today*, 2000, 59, 365-371.
165. R. M. Koros and E. J. Nowak, *Chem Eng Sci*, 1967, 22, 470-&.
166. R. J. Madon and M. Boudart, *Ind Eng Chem Fund*, 1982, 21, 438-447.
167. O. Krocher and M. Elsener, *Ind Eng Chem Res*, 2008, 47, 8588-8593.
168. A. Grossale, I. Nova, E. Tronconi, D. Chatterjee and M. Weibel, *Top Catal*, 2009, 52, 1837-1841.
169. M. Colombo, I. Nova and E. Tronconi, *Catal Today*, 2010, 151, 223-230.
170. P. S. Metkar, N. Salazar, R. Muncrief, V. Balakotaiah and M. P. Harold, *Appl Catal B-Environ*, 2011, 104, 110-126.
171. P. S. Metkar, M. P. Harold and V. Balakotaiah, *Appl Catal B-Environ*, 2012, 111, 67-80.
172. M. Iwasaki, in *Urea-SCR Technology for deNOx After Treatment of Diesel Exhausts*, eds. I. Nova and E. Tronconi, Springer, New York, 2014, ch. 8, pp. 221-246.
173. S. T. Korhonen, D. W. Fickel, R. F. Lobo, B. M. Weckhuysen and A. M. Beale, *Chem Commun*, 2011, 47, 800-802.
174. J. S. McEwen, T. Anggara, W. F. Schneider, V. F. Kispersky, J. T. Miller, W. N. Delgass and F. H. Ribeiro, *Catal Today*, 2012, 184, 129-144.
175. H. Y. Zhu, J. H. Kwak, C. H. F. Peden and J. Szanyi, *Catal Today*, 2013, 205, 16-23.
176. T. Yu, T. Hao, D. Q. Fan, J. Wang, M. Q. Shen and W. Li, *J Phys Chem C*, 2014, 118, 6565-6575.
177. S. Brandenberger, O. Krocher, A. Tissler and R. Althoff, *Appl Catal B-Environ*, 2010, 95, 348-357.
178. J. Szanyi, J. H. Kwak, H. Y. Zhu and C. H. F. Peden, *Phys Chem Chem Phys*, 2013, 15, 2368-2380.

179. R. Q. Zhang, J. S. McEwen, M. Kollar, F. Gao, Y. L. Wang, J. Szanyi and C. H. F. Peden, *Acs Catal*, 2014, 4, 4093-4105.
180. S. Malmberg, M. Votsmeier, J. Gieshoff, N. Soger, L. Mussmann, A. Schuler and A. Drochner, *Top Catal*, 2007, 42-43, 33-36.
181. I. Nova, M. Colombo, E. Tronconi, V. Schmeisser and M. Weibel, *SAE Technical paper* 2011, 2011-01-1319.
182. S. Kieger, G. Delahay, B. Coq and B. Neveu, *J Catal*, 1999, 183, 267-280.
183. Q. Sun, Z. X. Gao, H. Y. Chen and W. M. H. Sachtler, *J Catal*, 2001, 201, 89-99.
184. A. Grossale, I. Nova and E. Tronconi, *Catal Today*, 2008, 136, 18-27.
185. O. Krocher, M. Devadas, M. Elsener, A. Wokaun, N. Soger, M. Pfeifer, Y. Demel and L. Mussmann, *Appl Catal B-Environ*, 2006, 66, 208-216.
186. M. Colombo, I. Nova and E. Tronconi, *Catal Today*, 2010, 151, 223-230.
187. R. Nedyalkova, K. Kamasamudram, N. W. Currier, J. H. Li, A. Yezerets and L. Olsson, *J Catal*, 2013, 299, 101-108.
188. M. Inomata, A. Miyamoto and Y. Murakami, *J Catal*, 1980, 62, 140-148.
189. M. Kantcheva, V. Bushev and D. Klissurski, *J Catal*, 1994, 145, 96-106.
190. R. Q. Long and R. T. Yang, *J Catal*, 2002, 207, 224-231.
191. T. Yu, J. Wang, M. Q. Shen and W. Li, *Catal Sci Technol*, 2013, 3, 3234-3241.
192. T. Yu, D. Q. Fan, T. Hao, J. Wang, M. Q. Shen and W. Li, *Chem Eng J*, 2014, 243, 159-168.
193. F. Gao, M. Kollar, Y. L. Wang, J. Szanyi and C. H. F. Peden, unpublished work.
194. M. Schwidder, M. S. Kumar, U. Bentrup, J. Perez-Ramirez, A. Bruckner and W. Grunert, *Micropor Mesopor Mat*, 2008, 111, 124-133.
195. S. Brandenberger, O. Krocher, A. Wokaun, A. Tissler and R. Althoff, *J Catal*, 2009, 268, 297-306.
196. M. Devadas, O. Krocher, M. Elsener, A. Wokaun, N. Soger, M. Pfeifer, Y. Demel and L. Mussmann, *Appl Catal B-Environ*, 2006, 67, 187-196.
197. H. Y. Chen, Q. Sun, B. Wen, Y. H. Yeom, E. Weitz and W. M. H. Sachtler, *Catal Today*, 2004, 96, 1-10.
198. A. Grossale, I. Nova, E. Tronconi, D. Chatterjee and M. Weibel, *Top Catal*, 2009, 52, 1837-1841.
199. A. Grossale, I. Nova and E. Tronconi, *Catal Lett*, 2009, 130, 525-531.
200. P. Forzatti, I. Nova and E. Tronconi, *Angew Chem Int Edit*, 2009, 48, 8366-8368.
201. J. H. Kwak, D. Tran, S. D. Burton, J. Szanyi, J. H. Lee and C. H. F. Peden, *J Catal*, 2012, 287, 203-209.
202. P. N. R. Vennestrom, T. V. W. Janssens, A. Kustov, M. Grill, A. Puig-Molina, L. F. Lundegaard, R. R. Tiruvalam, P. Concepcion and A. Corma, *J Catal*, 2014, 309, 477-490.
203. Y. J. Kim, J. K. Lee, K. M. Min, S. B. Hong, I. S. Nam and B. K. Cho, *J Catal*, 2014, 311, 447-457.
204. M. Zammit, C. L. DiMaggio, C. H. Kim, C. K. Lambert, G. G. Muntean, C. H. F. Peden, J. E. Parks and K. Howden, *Future Automotive Aftertreatment Solutions: The 150 oC Challenge Workshop Report*, U.S. Drive Report, Southfield, MI, 2013.
205. T. Bogere, in *Urea-SCR Technology for de-NOx Aftertreatment of Diesel Exhaust*, eds. I. Nova and E. Tronconi, Springer Science and Busines Media, New York, 2014, pp. 623-655.
206. R. Chal, C. Gérardin, M. Bulut and S. van Donk, *ChemCatChem*, 2011, 3, 67-81.
207. S. van Donk, A. H. Janssen, J. H. Bitter and K. P. de Jong, *Catalysis Reviews*, 2003, 45, 297-319.
208. R. Floyd, L. Michael and z. Shaikh, in *Urea-SCR Technology for de-NOx Aftertreatment of Diesel Exhaust* eds. I. Nova and E. Tronconi, Springer Science and Business Media, New York, 2014, pp. 355-483.
209. D. Peitz, A. Bernhard and O. Krocher, in *Urea-SCR Technology for de-NOx Aftertreatment of Diesel Exhaust*, eds. I. Nova and E. Tronconi, Springer Science and Business Meida, New York, 2014, pp. 485-506.

210. J. Kwak, D. Tran, J. Szanyi, C. F. Peden and J. Lee, *Catal Lett*, 2012, 142, 295-301.
211. F. Gao, Y. L. Wang, M. Kollar, J. Szanyi and C. H. F. Peden, *Provisional Patent filed*, 2014, #30561-E.